Published in final edited form as:
Evol Biol. 2012 September 1; 39(3): 419–439. doi:10.1007/s11692-012-9159-6.

The Measurement of Local Variation in Shape

Eladio J. Márquez,
Department of Biological Science, Florida State University, Tallahassee, FL 32306, USA

Ryan Cabeen,
Department of Neurology, UCLA School of Medicine, Los Angeles, CA 90095, USA

Roger P. Woods, and
Department of Neurology, UCLA School of Medicine, Los Angeles, CA 90095, USA

David Houle
Department of Biological Science, Florida State University, Tallahassee, FL 32306, USA

Eladio J. Márquez: emarquez@bio.fsu.edu

Abstract

Geometric morphometrics comprises tools for measuring and analyzing shape as captured by an entire set of landmark configurations. Many interesting questions in evolutionary, genetic, and developmental research, however, are only meaningful at a local level, where a focus on “parts” or “traits” takes priority over properties of wholes. To study variational properties of such traits, current approaches partition configurations into subsets of landmarks which are then studied separately. This approach is unable to fully capture both variational and spatial characteristics of these subsets because interpretability of shape differences is context-dependent. Landmarks omitted from a partition usually contain information about that partition’s shape. We present an interpolation-based approach that can be used to model shape differences at a local, infinitesimal level as a function of information available globally. This approach belongs in a large family of methods that see shape differences as continuous “fields” spanning an entire structure, for which landmarks serve as reference parameters rather than as data. We show, via analyses of simulated and real data, how interpolation models provide a more accurate representation of regional shapes than partitioned data. A key difference of this interpolation approach from current morphometric practice is that one must assume an explicit interpolation model, which in turn implies a particular kind of behavior of the regions between landmarks. This choice presents novel methodological challenges, but also an opportunity to incorporate and test biomechanical models that have sought to explain tissue-level processes underlying the generation of morphological shape.

Keywords

Geometric morphometrics; Thin-plate splines; Shape variables; Interpolation; Local shape variation; Modularity; Biomechanical models

Introduction

Evolutionary studies of morphological form seek to address both questions about global properties of forms, and questions about local variation within larger forms. Global applications include group classification studies based on general properties of the

Correspondence to: Eladio J. Márquez, emarquez@bio.fsu.edu.

phenotype, such as phylogenetic reconstructions (e.g., Cardini 2003; Caumul and Polly 2005; Catalano et al. 2010; Klingenberg and Gidaszweski 2010), genetic association studies of whole-organ shape (e.g., Dworkin and Gibson 2006; Leamy et al. 2008), as well as analyses of global variational properties of morphological features, such as morphological integration (e.g., Cheverud et al. 1989; Wagner 1990; Marroig and Cheverud 2001; Young and Badyaev 2006; Ackermann 2009; Richstmeier and DeLeon 2009) and dimensionality (e.g., Mezey and Houle 2005; Hine and Blows 2006). Questions about local form focus on patterns of variation of specific traits. These include modularity and integration within complex organs (e.g., Mitteroecker and Bookstein 2007; Klingenberg 2008; Zelditch et al. 2009; Monteiro and Nogueira 2010), genetic association studies of discrete multivariate traits (e.g., Cheverud et al. 1991; Atchley et al. 1992; Leamy et al. 1999; Mezey et al. 2000; Zimmerman et al. 2000), and definition of morphometric characters for cladistic analysis (MacLeod 2002; González-José et al. 2008). An increasingly important class of applications attempt to interpret local shape variation in terms of the genetic and developmental processes responsible for shaping morphology (e.g., see Hallgrímsson et al. 2009; Klingenberg 2010). Those processes can themselves be characterized by their spatial location, demanding models built upon local aspects of shape.

Landmark-based geometric morphometrics makes explicit use of spatial information to allow the definition, measurement and analysis of the shape of whole landmark configurations (Bookstein 1992). It is therefore ideally suited to answer the first category listed: questions about global forms. This is done by directly using untransformed landmark coordinates (e.g., Workman et al. 2002; Leamy et al. 2008; Márquez 2008), scores on an orthogonal basis (e.g., principal components or uniform plus non-uniform partial warp scores; e.g., Zimmerman et al. 2000; Dworkin and Gibson 2006; Stelkens et al. 2009), or subsets of principal components (e.g., Mezey et al. 2005; Burgio et al. 2009; Feng et al. 2009). Multivariate methods can be used to find directions in phenotype space that are most associated with particular hypotheses. For example, one can ask which directions in shape space are most affected by genotypic differences (e.g., Haley and Knott 1992; Leamy et al. 1999; Klingenberg et al. 2001).

These global approaches have the important shortcoming that dealing with whole configurations precludes focusing on specific local traits, such as the shape of a region known a priori to be affected by a particular developmental event. When our aim is to uncover genetic determinants of phenotypic traits, we need analytical approaches that accommodate defining traits a priori, as in univariate genotypic association studies. Current geometric morphometric approaches, however, can only be applied uneasily and heuristically to questions about local variation. Shape is a multivariate property of the form which is contained in the relationship between changes at all landmarks (Zelditch et al. 2004). Landmark superimposition spreads local differences over the whole shape, making it necessary to consider all landmarks in a configuration in order to quantify these differences (Woods 2003).

Non-geometric measures of form, such as lengths or areas can capture local information by virtue of referring explicitly to a region, rather than the whole. Given this easy precedent for defining local as what is measured in a region, those using geometric morphometrics have sometimes succumbed to the temptation to treat landmarks directly as traits in quantitative analyses. Consider one naïve method for capturing local shape variation—the use of variation at a single landmark to make inferences about local changes in form (e.g., Albert et al. 2008; Catalano et al. 2010). It is readily apparent to most practitioners that such individual landmarks lose almost all information about shape, for reasons we discuss in more detail below. We demonstrate here that analysis of subsets of landmarks within a form similarly gives only distorted information about local shape and shape variation.

Nevertheless, the practice of using subsets of landmarks to indicate local variation is widespread. This approach has been used in genetic association studies in the Drosophila wing (Zimmerman et al. 2000; Dworkin et al. 2005; Feng et al. 2009; Klingenberg 2009), phylogenetic reconstructions of cranial evolution in *Homo* (González-José et al. 2008), and in analyses of morphological integration of the rodent mandible (Klingenberg et al. 2003; Monteiro et al. 2005; Zelditch et al. 2009).

We propose that local shape differences can be better characterized through the use of interpolation functions that predict changes at any point on the form from the entire set of sampled points. Interpolation is widely used as a visualization tool now, so what we advocate is a change in perspective, rather than a radical departure from current practice. The change is to view the results of interpolation as data, based on a testable hypothesis about the nature of the local deformations that distinguish two forms. Using interpolation results in this way requires that the interpolation model assumes a key position in our analysis. Consequently, it seems appropriate to treat any particular interpretation of a regional deformation as but one among many alternative hypotheses. By expressing such changes in terms of models, we emphasize the fact that there are assumptions associated with any representation of deformation based on discrete landmarks, and thus it seems logical to make these assumptions explicit. Ultimately by tailoring our interpolation models to experimentally observed developmental changes in shape, for example through spatial heterogeneity of growth rates under mechanical stress (Rauzi et al. 2008; Aigouy et al. 2010), we can hope to infer something about the processes that give rise to a more general set of changes in form. In this contribution, we discuss criteria for selection of continuous interpolation functions in addition to methods to evaluate these functions at corresponding (e.g., homologous) spatial locations.

Measurement of shape

In geometric morphometrics, shapes of individual landmark configurations are usually encoded as shape variables measuring deviations from a reference shape. The two most popular choices for such variables are Procrustes residuals and partial warp scores (Dryden and Mardia 1998). Procrustes residuals (PR) are landmark-wise differentials between individual shapes and an optimally computed shape mean or “atlas.” Partial warp scores (PW) are directions of shape variation extracted from a basis defined with respect to the degree of localness (i.e., bending energy) associated with the space of possible deformations that a reference configuration can undergo (Bookstein 1992). Both shape variables occupy a space nearly identical to a Euclidean space tangent to the actual shape space at the atlas (Rohlf 1999), closely satisfying both the non-Euclidean geometry of shape differences and the Euclidean geometry underlying ordinary multivariate statistical analyses.

Of these two types of variables, PR invite defining traits as subsets of landmarks because they denote a specific location, and thus are a natural choice in studies that require a priori definition of traits. An often overlooked consequence of using PR, however, is the fact that an entire configuration of landmarks is required to describe a single high-dimensional observation in shape space (Woods 2003). Shape deformations can only be measured by PR to the extent that *all* residuals are used in any particular analysis; No subset of landmarks can capture only local variation. This is partly because superimposition induces auto-correlations among landmarks within configurations (Bookstein 1992), hence distributing both global and local information (including measurement error) over the entire set of residuals (Walker 2000; van der Linde and Houle 2009), but more fundamentally because interpretability, and hence measurement of shape variation at a local region, depends on the pattern of variation at neighboring regions.

Context-dependence of shape differences arises because the proper interpretation of landmark displacement in a region of interest depends on the pattern of displacement of other landmarks. This spatial dependence is exemplified in Fig. 1 with a hypothetical deformation of a Drosophila wing relative to a reference configuration. The fact that landmarks in the region labeled as **a** all have large PR might suggest that the region is undergoing a shape change. For example, treating the landmarks along vein L1 as a partition might suggest that the region adjacent to L1 had changed. However, in the context of the whole wing, the fact that all the landmarks in region **a** move in the same direction suggests that a more appropriate interpretation is that region **a** is being displaced by changes in region **b**, and that this displacement preserves the shape of region **a**. The boundary between regions **a** and **b** in Fig. 1 in fact lies close to an important developmental boundary laid down early in wing development. A pattern of change like that depicted would have plausible interpretations in terms of differences in growth confined to the posterior compartment.

Defining Localness

Our interest is in approaches that allow us to estimate variational properties of specific morphological regions selected a priori as subsets of larger structures. We refer to these regions as **focal** traits (e.g., McGuigan and Blows 2010) to emphasize the fact that they are chosen to address specific questions instead of being derived from algorithms unrelated to these questions, such as principal components or partial warps. We can break down changes in focal traits further into changes at points within each region. We refer to these infinitesimal contributions to shape deformation as **local** (e.g., Cheverud et al. 1991; Atchley et al. 1992). These changes are inferred by application of an interpolation function to the landmark data. This assumes that deformation information has ergodic properties over the whole structure under analysis.

This notion of localness differs from the concept of non-affine deformations (e.g., Bookstein 1992), which result from decomposing the difference in shape between two configurations into a global (i.e., affine) component with uniform direction of shape change, and a local (i.e., non-affine) one estimated as a residual from this global trend. This residual has been minimized as a roughness penalty during interpolation, and is uniquely defined, and thus potentially distinct, at each local region of the shape. It is possible to define focal traits based exclusively on non-affine variation; however, there is no reason to assume distinct biological bases for affine versus non-affine components of shape change.

Estimation of Local Shape Variation

Given an anatomical structure represented by a collection of landmarks, we wish to estimate phenotypic variation of the shape of a focal region in relation to factors such as genotype or environment. The estimation of local shape variation comprises two related methodological problems, i.e., estimating shape deformations at arbitrary regions in a single individual, and ensuring that these measurements are comparable across individuals. Thus, the procedure for extraction of local shape data consists of three basic elements, namely (1) a shape deformation function, (2) a discretization (i.e., evaluation) method, and (3) criteria for choosing evaluation sites.

The following sections briefly explore each of these elements. Each one can be approached in multiple ways, and the appropriate choice may well vary with the biological question motivating a particular study. For example, when choosing a deformation function, we anticipate that models appropriate for the type of tissue (e.g., epithelium, mesenchyme, cartilage, dermal bone) and process (e.g., morphogenesis, growth, remodeling, regeneration) under analysis can be developed (Humphrey 2003; Holden 2008). Similarly, spatial models

can be evaluated as local deformations using tensors, vectors, or area measurements depending on the type of data at hand, whereas the choice of evaluation sites should be based on inferences about homology, for which different criteria may apply in different situations.

Shape Deformation Functions

Shape deformation functions allow the prediction of local changes that distinguish two forms based on a sampled set of locations on those forms, such as landmarks and semi-landmarks. Generally, these functions interpolate deformations by weighting changes observed at these sampled locations according to their distance to a point of interest. These weights, in turn, can be defined ad hoc or derived from a model describing the differences between two landmark configurations as deformations of a physical object. Deformations inferred in this way are often represented graphically through deformation of regular grids (Fig. 2a; Dryden and Mardia 1998). We consider four general classes of deformation functions, namely interpolating splines, smoothing splines, kriging, and finite elements. We briefly describe their basic aims and properties here, and consider them in more detail in the Appendix, which shows the close mathematical relationships among these methods.

Interpolating Splines—Interpolating splines use the spatial locations of a set of landmark points (or curves) to map arbitrary locations in a reference configuration onto corresponding locations in a target form (Woods 2003). In the process, differences among neighboring landmarks are smoothed according to an optimal function so that interpolated sites receive greater influence from nearer landmarks than from more distant ones. One set of interpolating functions that are widely used in geometric morphometrics are thin-plate splines (TPS; Bookstein 1992). TPS model deformations using the physical analogy of the bending of a thin metal plate, and produce the smoothest possible deformation of a configuration of 2-D coordinates onto another (Bookstein 1992; Dryden and Mardia 1998; Zelditch et al. 2004). According to this model, deformations that are more global in scope tend to be favored due to their lower contribution to the total bending energy than deformations between nearby landmarks. Alternative interpolation functions are derived from a variety of solid and fluid dynamics models (Holden 2008), such as elastic body splines (Davis et al. 1995, 1997), or by modifying existing functions to control for the influence of local deformations on interpolated values, such as done by Approximating or Gaussian TPS (Rohr et al. 2001). We have chosen to use TPS throughout this paper due to their familiarity, but would nevertheless like to emphasize that there are alternative models, some of which are potentially more appropriate for biological problems.

Smoothing Splines—Smoothing splines generalize interpolating splines in assuming that landmarks are measured with error. The goal of the smoothing is to minimize the impact of that error on computation of the splines (Hutchinson and Gessler 1994). Smoothing splines can also be used to test among alternative interpolation functions.

Kriging—Kriging is a method commonly used in geostatistical analysis to predict the value of a variable at an arbitrary site from values of the same variable measured in a set of adjacent sampled sites (Laslett 1994). Kriging assumes an underlying random field that determines the spatial distribution of the variable of interest, including values observed at sampled sites as well as at all unobserved sites in between them (Matheron 1973; Schabenberger and Gotway 2005). Predicted values are obtained as weighted sums of observed values, and the weights chosen to minimize mean prediction error (Goovaerts 1997). An underlying function is chosen to model the information decay with distance between sampled and predicted values, but this function is generally not chosen to model deformations of a rigid set of points, as done by interpolating splines.

Finite Element Methods—Finite element methods (FEM) predict local values within rigid polygons or polyhedrons—the finite elements—from changes observed at their vertices (e.g., Lewis et al. 1980). FEM subdivide a landmark configuration into similar elements and thus interpolation is not based on a global function as in methods described above. Within elements, different approaches assume changes to be uniform or modeled using a function with both uniform and non-uniform components (Bookstein 1986; Lewis et al. 1980; Cheverud et al. 1983).

These descriptions suggest that these four methods represent alternative solutions motivated by the same problems, i.e., prediction or estimation of unknown values given a spatial distribution of samples. The Appendix further shows that commonalities among these techniques are also reflected also in their mathematical formulations, whereby smoothing splines generalize interpolating splines; interpolating splines are indistinguishable from kriging under certain circumstances; and FEM can be used as a spatially discrete implementation of spline functions.

Local Evaluation of Interpolation Functions

In order to obtain a discrete representation of a deformation, an interpolation function must be evaluated at a focal point, where partial derivatives can be used to define various shape descriptors (Woods 2003). These descriptors are applicable wherever an explicit derivable deformation function is available, but equivalent measurements could be obtained in most cases through numerical differentiation.

Consider a general function d mapping the point $\mathbf{p}$: x, y, z anywhere in a reference shape into a corresponding point $d(\mathbf{p})$ in a target shape,

$$d(\mathbf{p}) = \sum_{j}^{h} \beta_j U_j(\mathbf{p}) + \sum_{i}^{k} \alpha_i F(\mathbf{r}_i) \quad (1)$$

where U and F are polynomials describing the affine and non-affine components of the deformation, respectively, $\mathbf{r}_i$ is the distance between $\mathbf{p}$ and the ith sampled landmark in the reference configuration, and α and β are estimable parameters. Direct application of Eqn. 1, which generalizes Eqns. 5 and 10 (from Appendix), yields a vector of bi- or trivariate splines (or vector fields) denoted by $d(\mathbf{p}) = [d_x, d_y]^T$ or $d(\mathbf{p}) = [d_x, d_y, d_z]^T$, respectively, which describe shape deformation near a focal point while incorporating information from elsewhere in a configuration. Applied to nodes in a regular sparse grid, these splines can be used to produce deformation plots (Fig. 2a). Alternatively, functions can be visualized as approximately continuous vector fields (Fig. 2b) to obtain a better resolved representation of the spatial distribution of deformations implied by a model. In either case, point values are computed using a spline function, which, like sampled landmarks or residuals, cannot be construed as shape variables, inasmuch as each describes deformation contributions at a point, shape being a property of 2- or 3-D regions instead.

A second discrete representation is given by the Jacobian matrix $J_{xyz} = \frac{\partial(d_x, d_y, d_z)}{\partial(x,y,z)}$, which maps infinitesimal deformations between reference and target configurations by measuring the rate of shape deformation at any point along all directions simultaneously, so that

$$d(\mathbf{p}) \approx d(\mathbf{q}) + J_{d(\mathbf{q})} \cdot (\mathbf{p} - \mathbf{q})$$

where **q** and $d(\mathbf{q})$ are sampled landmarks at a reference configuration and their corresponding deformed positions (i.e., at the target configuration), respectively (Woods 2003). The accuracy of this approximation is a decaying function of the distance between corresponding points, increasing monotonically as $\|\mathbf{p} - \mathbf{q}\| \to 0$. Notice that since J contains the first partial derivatives of d, the affine component U, which is a first-order polynomial of **p**, becomes a constant; therefore, J captures local information as localized variation in the non-affine component of the deformation. The interpretability of the first partial derivatives of $d(\mathbf{p})$ is ensured by the fact that the inferred pattern of spatial variation has been optimized during interpolation upon minimization of the roughness penalty (Eqns. 3, 4), computed using the second derivative of $d(\mathbf{p})$.

For the 2- and 3-D cases, Jacobian matrices are given respectively by

$$J_{xy} = \begin{bmatrix} \partial d_x/\partial x & \partial d_y/\partial x \\ \partial d_x/\partial y & \partial d_y/\partial y \end{bmatrix}$$
$$J_{xyz} = \begin{bmatrix} \partial d_x/\partial x & \partial d_y/\partial x & \partial d_z/\partial x \\ \partial d_x/\partial y & \partial d_y/\partial y & \partial d_z/\partial y \\ \partial d_x/\partial z & \partial d_y/\partial z & \partial d_z/\partial z \end{bmatrix} \quad (2)$$

Each Jacobian matrix can be directly treated as a shape variable describing local deformation at an arbitrary point, unlike splines or landmarks. Jacobians can be registered and mapped onto a Euclidean space, tangent to a shape manifold at the mean Jacobian (Woods 2003).

A Jacobian matrix gives information about the change in shape deformation with respect to the direction of deviation from the focal point, requiring a minimum of four and nine vectors to characterize local variation at one point in 2- and 3-D, respectively. This poses a challenge in that it could lead to an excessive number of variables for any modestly sized shape. For many purposes, however, lower dimensional representations of J should provide an adequate summary of the influence of observed residuals on neighboring regions. Two such representations that retain interpretability are the determinant and the principal eigentensors of J, which provide, respectively, univariate and two- or three-variate measures of local shape change (Woods 2003; Commonwick et al. 2005).

Jacobian determinants are, for most practical applications, apt estimators of local shape deformations. If topology is preserved between source and target configurations (i.e., there are no flips or reversals in the relative position of landmarks), these determinants are positive and represent relative change in surface area (2-D) or volume (3-D) in the region about the interpolation point. Thus, $\det J_{\mathbf{p}} = 1$ indicates absence of area/volume change around point **p**, so that only area/volume-preserving shears have occurred; similarly, $\det J_{\mathbf{p}} = 2$ indicates that local area/volume is doubled, and $\det J_{\mathbf{p}} = 0.5$ indicates that local area/volume is halved. To project these estimators onto a tangent space for statistical analysis, it suffices to use the logarithm of the determinant after Jacobian matrices have been centered at the identity matrices, i.e., deformations are quantified relative to a reference mean (Woods 2003). Replacing J by its determinant transforms the local deformation information into a scalar field (Fig. 2c, d), consequently causing loss of information about the geometry of local shape change which can be compensated for by using a sufficiently dense distribution of Jacobians. Figure 2c illustrates the same deformation information shown in Fig. 2a, b, represented in terms of logarithms of Jacobian determinants from spline functions. Notice that the scalar field represented here provides readily interpretable information regarding the distribution of shape differences. Furthermore, local changes in areas (Fig. 2c) are readily referable to biological processes while local velocity vectors (Fig. 2b) are not.

Local Correspondence Among Configurations

To ensure the meaningfulness of comparisons between forms, the points where interpolation functions are evaluated should be chosen to maximize their biological correspondence throughout a sample. In visualization applications, functions are typically evaluated at nodes of regular or biorthogonal grids (Fig. 2a; Bookstein 1986; Dryden and Mardia 1998), rather than according to their anatomical correspondence or homology. On the other hand, landmarks (and semi-landmarks) are normally chosen to maximize correspondence and ensure comparability. Criteria for discretization should be a function of known or predicted (Boyer et al. 2011) landmark locations. Delaunay triangulation is a useful algorithm for choosing sets of internal (non-landmark) nodes based on adjacency rules among landmarks (Dryden and Mardia 1998). Given the uniqueness of the triangulation, which holds as long as no three landmarks are co-linear and no four landmarks lie on the same circle, triangle vertices are comparable across specimens, much like the original landmarks and semi-landmarks. One way triangulation patterns can then be used to choose interpolation points consists of selecting one of the triangle centers (e.g., incenter, circumcenter, Voronoi vertices, centroid) as an evaluation point (Fig. 3a). These points, in turn, can be incorporated as vertices for further triangulation iterations, allowing the generation of sampling schemes of potentially unlimited resolution (Fig. 3b). Figure 2d illustrates this approach by evaluating the same function and data shown in Figs. 2a–c, at centroids of triangles generated by one triangulation round on the original landmarks (i.e., closed circles in Fig. 3b). These scalar values convey local deformation information at points which are arguably comparable across configurations.

The Analysis of Local Shape Variation: Examples

Case Study: Ability of Landmark- Versus Interpolation-Based Methods to Recover a Simulated Pattern of Variation in the Drosophila Wing

The following examples illustrate how this system for treating interpolation results as data can be used in some simple cases. They also show the inability of landmark data alone to capture focal shape variation in a consistent manner. Patterns of shape variation were simulated to represent scenarios where obvious focal shape differences occur despite relative constancy in magnitude of landmark (i.e., Procrustes) residuals. These simulations also illustrate some differences between the two available alternatives for extracting landmark partitions to study focal shape variation, namely simultaneous alignment, where subsets of landmarks are directly partitioned out from pre-shapes without further alignment, and separate alignment, where subsets of landmarks are re-registered after being partitioned (Klingenberg 2009).

Simulation Method—Simulations were used to recreate data conforming to a main effects model (i.e., MANOVA), consisting of a linear effect representing the difference between the means of two groups of Drosophila wings, such as might be caused by single-nucleotide polymorphisms (SNPs; e.g., Ayroles et al. 2009; Yang et al. 2011). Main-effect vectors were chosen to match features (see Fig. 4) suggested by our unpublished data on genotypic differences in the Drosophila Genetic Reference Panel (DGRP; Baylor College of Medicine/Human Genome Sequencing Center 2010). Two vectors, v_1 and v_2, were produced in this manner, one describing a wing shape with invariant anterior compartment and highly variable posterior one (Fig. 4a), and another, identical except for a focal reflection of variation along one vein to produce wings where both compartments are highly variable (Fig. 4b). Corresponding mean vectors for two groups lying at opposing extremes of these vectors were defined as $0.5v_i$ and $-0.5v_i$; these vectors were then used to generate random samples of 1,000 sets of 200 vectors (i.e., 100 per group) from a multivariate normal

distribution with error covariance matrices equal to the P matrix of 165 of the DGRP lines (J. Nye, unpublished observations).

Simulated configurations comprise 44 Procrustes-aligned landmarks and semi-landmarks, from which residuals were computed and used as shape variables. Interpolated values were computed as the base-2 logarithm of the determinant of the Jacobian of a TPS function evaluated at specific wing locations. These points were located at the centroid of triangles obtained from a Delaunay triangulation derived from 12 Type I landmarks defined at wing vein intersections. Landmark and interpolated data were compared in terms of their ability to recover simulated deformation scenarios using multivariate (i.e., MANOVA) and spatially-explicit univariate (i.e., ANOVA) statistics.

Results

Figure 4a, b depict the two effect vectors used for simulations, both as landmark differentials and as TPS interpolations of local deformations. These heat maps are useful visual aids for the interpretation of local effects of landmark variation, and are produced by cubic interpolation of the TPS-interpolated Jacobians based on a high-resolution grid overlaid on the entire wing surface. Comparisons of landmark versus interpolated data are focused on the wing regions with more pronounced effects in simulations. These correspond to the portion of the wing anterior to the longitudinal vein that is closest to the anterior margin, i.e., L2 (see Fig. 1 for vein nomenclature), and the portion bound by longitudinal veins L4 and L5, spanning the anterior portion of the posterior wing compartment.

As expected, effect vectors account for over 99% of the variation of whole configurations in both scenarios, using both types of variables (Table 1). In contrast, patterns of focal shape variation differ between interpolated and landmark data in the two regions of interest, namely L2 and L4–L5, depending on deformation scenario and partitioning method (Table 1). Specifically, within the L4–L5 region about 100 and 97% of the variation in landmark and Jacobian data, respectively, is explained by the main group effect, irrespective of whether partitions are realigned (Table 1). In contrast, in the L2 region only about 28% of variation of interpolated values is explained by this effect in scenario I and 97% in scenario II, consistent with the conditions of the simulation. Landmark data shows a highly significant effect in the L2 region in both scenarios, with differences between group means explaining over 98% of the variation in all cases.

Despite the similarity between patterns of multivariate variation of original and realigned landmark data, the latter approach can approximately recover patterns of shape variation if the correct set of points is selected as a partition. Thus, separately aligning L2 and L4–L5 configurations approximately recovers the shape differences simulated in both scenarios (Fig. 5a, b). Such contrast between alignment schemes results from the removal of non-shape variation during the re-superimposition of subsets of landmarks, suggesting partition realignment as a preferred approach for capturing focal shape information. This advantage of realignment, however, is somewhat offset by the loss of contextual information essential for proper interpretation of shape differences. This becomes apparent by comparing landmarks associated to the L2 region in Figs. 4b and 5b, which highlight the tendency of superimposition to re-distribute variation among landmarks, favoring their evenness, and potentially leading to distorted interpretations of local deformations. This tendency is particularly problematic whenever landmark variation is non-uniformly distributed across a partition, where alignment would favor a transfer of variation from highly variable regions to those with low variation (Walker 2000).

Interpolated values integrate information from the whole configuration when producing local estimates, and thus can in principle be treated as individual variables that can be used

in multivariate analyses as focal estimates of shape change, or in univariate analyses for the purpose of spatial localization of shape differences. Figure 6 maps R^2 and P values from individual Jacobian-based ANOVAs onto a reference wing, producing an informative representation to assist in identifying the approximate spatial distribution of differences between the mean shapes of two groups.

Interestingly, some heterogeneity in these values is apparent throughout otherwise homogeneous regions (e.g., notice low P values within region L2 from scenario I). This is a consequence of the underlying interpolant being a continuous function, sensitive to fluctuations in available parameters (i.e., landmarks), suggesting that increased sampling of landmarks may be valuable. Figure 7 illustrates how an increase in semi-landmark sampling might help local estimates become increasingly stable. There is a larger difference in the results when increasing the number of points by a factor of 2 and 4, than when it increases between 4 and 8, suggesting that interpolation quality improves non-linearly with the amount of sampling.

Case Study: Analysis of Patterns of Covariation Among Partitions of the Rodent Mandible

The rodent mandible constitutes a model system for the study of patterns of covariation among morphological regions (Zelditch et al. 2008). Many such studies reference a developmental and genetic model that postulates that the variational properties of the fully developed mandible derive ultimately from the physical aggregation of modular mesenchymal condensations, which develop as independent units in early embryos (Atchley and Hall 1991; Hall and Miyake 2000). Directly applied, this model generates an expectation of modular variation that can be tested against plausible alternatives, incorporating, for instance, effects of reorganizing agents that become relevant later in development, such as mechanical loading and stress (Zelditch et al. 2008). Expectations of modular variation are often represented as alternative partitions of the same morphological variables, which are mutually tested for support (Klingen-berg et al. 2003; Monteiro et al. 2005, Márquez 2008). In geometric morphometrics methodology, this procedure entails partitioning landmark configurations into subsets of landmarks, and available methods focus on the multivariate structure of covariation among partitions (e.g., Mitteroecker and Bookstein 2007; Martínez-Abadías et al. 2009), scalar measurements of partition correlation (e.g., Monteiro et al. 2005; Klingenberg 2009), or the global structure of covariation (Richtsmeier et al. 2005; Márquez 2008).

As an example, we analyzed a sample of adult specimens from three Sigmodontine rodent species, namely *Nectomys squamipes* (NS, N = 70), *Holochilus chacarius* (HC, N = 67), and *Microryzomys minutus* (MM, N = 53). These samples belong to a larger study of morphological integration of the rodent skull (Márquez 2008), and span substantial ecophenotypic variation, comprising species dwelling in similar environments but with different feeding ecologies (NS vs. HC and MM), as well as species at different ends of the size spectrum of Muroid rodents in general (NS and HC vs. MM).

A total of 18 landmarks and 51 semi-landmarks were used to parameterize a TPS function whose Jacobians were then evaluated at the centroids of unique sets of triangles found by Delaunay tessellation. A scalar field of local area changes was then computed as the base-2 logarithm of the determinant of these Jacobians, consisting of 86 points located inside the mandible area (Fig. 8). Differences among the three species are supported by MANOVA based on full-configuration data using both landmark (Wilks $\Lambda = 0.0001$, $P \approx 0$) and interpolated data (Wilks $\Lambda = 0.0002$, $P \approx 0$).

Regions mapping developmental modules onto the adult mandible were defined and assigned non-overlapping sets of landmarks and semi-landmarks. For illustrative purposes,

and without loss of generality, six regions were defined, spanning, respectively, (1) the distal (i.e., masticatory) portion of the incisor alveolus (IN), (2) the molar alveolus (ML), (3) the "ramus," including the insertion site for the medial masseter as well as the proximal portion of the incisor alveolus (MS), (4) the coronoid process (CR), (5) the condyloid process (CN), and (6) the angular process (AN) (Fig. 8). Partition-based analyses were carried out to investigate differences between landmark- and interpolation-based approaches in studies of patterns of focal shape variation and covariation.

Pairwise differences among species, quantified as vector differences, were computed using both whole configurations and separate partitions. Interpolation-based estimates are always based on whole configurations, and thus values are invariant with respect to partition schemes (Fig. 9). In contrast, interspecific differences computed using landmark partitions appear distorted relative to whole configurations (Fig. 10a), mainly due to the absence of contextual information regardless of whether partitions are realigned (Fig. 10b, c). This is not surprising, given that the landmarks in the mandible do not define closed shapes, but fall only along some edges of the regions they represent. Proper reading of shape differences requires consideration of landmarks in adjacent partitions. Even though realignment would restore interpretability of landmark differences as local shape differences, neither approach can successfully capture both local and relative shape information with respect to other partitions.

By assuming a continuous mapping of differences between configurations, it becomes possible to quantify local variation at arbitrary points using interpolated values. Scalar fields can thus be combined into regional vectors or simply treated as scalars (e.g., by averaging or adding them), in multivariate and univariate tests. An example is illustrated in Fig. 9, where results from multiple comparisons among NS, HC, and MM mandibles based on (univariate) Jacobian determinants are mapped on a mandible, providing an informative visualization for the spatial localization of interspecific differences. Note that in general, it is advisable to interpret these values jointly in the context of their spatial distribution. Such analyses could, however, help pinpoint atypically similar or dissimilar focal regions for further testing.

To examine the effect of choice of variable on patterns of intraspecific variation, we estimated variances of partitions as sums of Procrustes residual or Jacobian variances standardized by number of variables (i.e., landmarks or interpolation points). These variances, shown in Table 2, further suggest that these two types of variables measure different properties of the form. Within species, original and realigned landmark-based estimates of partition variation are positively correlated with each other (correlation coefficients are 0.97, 0.92, and 0.95 for NS, HC, and MM, respectively), and negatively correlated with Jacobian-based estimates (average correlation coefficients are −0.64, −0.41, and −0.18 for NS, HC, and MM, respectively). Similarly, estimates of variation across partitions are highly correlated among all species when computed based on landmarks (correlation coefficients range between 0.77 and 0.94 for original and between 0.84 and 0.95 for realigned landmarks), with masseteric and angular partitions showing consistently larger variances. In contrast, Jacobian-based estimates are highly correlated between NS and HC (r = 0.97), with condyloid, coronoid, and molar partitions being the most variable, but poorly correlated between MM and both NS (r = 0.29) and HC (r = 0.08).

This relatively higher capacity for species distinction by Jacobian data is echoed in patterns of covariation. A simple statistic for measuring covariation between two partitions is the RV-coefficient (Escoufier 1973; Márquez and Knowles 2007; Klingenberg 2009), which provides a multivariate analog to the correlation coefficient. Table 3 shows RV-coefficients among all partitions considered in this study. Overall, landmark-based RV-coefficients are low and homogeneous across partitions (range is [0.10, 0.31] for original and [0.07, 0.24]

for realigned partitions), whereas Jacobian-based coefficients display a wider range of values (range = [0.02, 0.58]), suggesting that Jacobians reveal more informative aspects of variation than landmark residuals.

The apparent ability of Jacobian data to produce stronger variation and covariation signals likely results from the integration of spatial information beyond the boundaries of fixed partitions. Partitions like the molar, coronoid, or masseteric, as defined herein, delineate particularly “open” outlines containing little information about their immediate surroundings. In contrast, closed compartments, such as vein-bounded cells in the Drosophila wing, should be largely sufficient to determine deformation patterns within those cells. This could explain why the large Jacobian-based correlation observed between molar and coronoid partitions in MM is not matched by landmark data (Table 3), as the signal for this correlation is enhanced by information provided by landmarks along the masseteric ridge, which defines a ventral margin of sorts for these partitions. Conversely, this could also explain why the angular partition, which lacks an equivalent closing boundary, is so poorly correlated with other partitions when using Jacobians, relative to landmarks, highlighting the fact that the quality of discrete evaluations of spatial functions depends largely on the density of sampled points in the vicinity of such evaluations.

Discussion

A Case for Local Estimates of Shape Variation

In landmark-based geometric methods, shape is an abstract concept defined as the property of the form that remains after removing non-shape information (e.g., Zelditch et al. 2004). Estimates of variation in shape of a structure are often based on landmark differentials. Anyone examining a pattern of such differentials will naturally try to infer an explanation for this variation based on what may have happened between the landmarks, such as local expansions and contractions. This process has largely been intuitive. We argue for making this process algorithmic, and tying it to explicit assumptions about the types of changes that are most likely to have occurred. We thus see interpolation, previously employed largely as a visualization tool, as generating data that can be used to make, and ultimately test, predictions about causes of differences in form. The resulting framework assumes that differences between forms captured by landmark residuals can be fit to a continuous function or family of functions inferred from the joint behavior of all landmarks.

When treated as whole structures, landmark configurations contain the same information as any interpolation function derived from them. Discrepancies emerge, however, among estimates of shape differences at local (i.e., infinitesimal) and focal (i.e., regional) scales, where the focus is on the behavior of regions spanning subsets of landmarks. Focal shape, as we have shown, is context-dependent in the sense that in order to adequately interpret focal deformations, we often require information present beyond the boundaries of the partition of interest. In general, interpretability of local deformations is potentially informed by all of the landmarks in a configuration.

Interpolation-based shape quantification assumes a particular form for this context-dependence. This approach can be seen as an extension of random vector field kriging methods used in geostatistical analysis for interpolation of local functions (Hutchinson and Gessler 1994; Laslett 1994), albeit with an emphasis on estimation of variation and model choice, shared with finite element methods (FEM; Lewis et al. 1980). Unlike FEM, which estimate shape and shape variation from pre-determined subsets of nearby landmarks, our approach makes use of all landmarks for such estimation. In the Appendix, we show that the entire family of methods available for predicting variation at arbitrary points on a form share great similarities, and in special cases are precisely equivalent.

Thus, landmark configurations can be fitted to continuous functions capable of spawning arbitrarily spaced fields of Jacobian matrices, spline vectors, or integrated scalars. A function-based approach offers flexibility of choosing among a variety of metrics that can yield readily interpretable scalar measurements, such as those used in Figs. 6 and 9. The logarithms of these scalars estimate proportional infinitesimal changes in local area and can be interpreted both as focal deformations, and as local contributions to regional variation.

A potential drawback of splines and kriging is that both methods assume global homogeneity of the processes underlying local variation. In kriging, a single homogeneous stochastic process is assumed to give rise to observed (and estimated) values, whereas a single function is normally used in spline-based interpolation. If the objective of interpolation is purely to smooth differences observed at landmarks, then it may be desirable to choose a single function, such as thin-plate splines (TPS). If, on the other hand, we wish to use interpolation as a tool for statistical estimation or prediction, then the guiding optimality principle should be framed in terms of hypotheses about of the processes underlying spatial variation. Our hypotheses may involve different models in different parts of the form. For instance, using a single function or stochastic process as the basis for interpolation usually implies assuming that spatial information is distributed isotropically around an interpolation point (Goovaerts 1997; Holden 2008), whereas in living tissues subcellular forces driving growth and development are highly anisotropic (Humphrey 2003; Rauzi et al. 2008). An apparent advantage of FEM over splines and kriging methods is that by partitioning a morphological structure into FEs, isotropy is only assumed for points within individual elements. Thus, framed in a hypothesis-testing context, FEM could in principle be used to compare among alternative partition schemes corresponding to specific predictions for spatial covariance structure, with FEs defining locally isotropic regions. Given that ordinary interpolation is used to obtain local values within FEs, it seems that such an approach could be seen as a quasi-discrete version of the random fields approach underlying splines, kriging, and related approaches (Matheron 1973; Grenander and Miller 1998), and it suggests that fitting instead a patchwork of local fields might be a useful alternative to incorporate spatial heterogeneity.

An interesting consequence of using interpolation-based methods concerns a shift in relevance of homology constraints. Landmark homology is often a primary consideration when establishing comparability across forms. Treating shape as a continuous function relaxes this constraint somewhat by requiring only homology of broad regions or whole configurations. Decisions such as the number of landmarks and semi-landmarks to sample and the number of interpolated points to evaluate can be based solely on practical criteria. Proper registration, however, remains a critical issue. Both registration and interpolation could in principle be done on deformation functions directly. At present, however, it remains unclear which functions can be empirically justified; for now, landmark homology is the best supported criterion to ensure meaningful registration of shapes.

The recursive triangulation approach we have used seeks to balance the need for discrete sampling on a continuous surface imposed by interpolation methods and the homology requirements imposed by registration. In practice, the number of measured sites is limited by sample size and computational demands, and thus it may often be useful to have criteria for prioritizing sampling locations in order to maximize the quantity and quality of information in a sample. Examples of such criteria include (1) preferring points that minimize redundancy across spatially adjacent regions within individuals, (2) emphasizing regions with the highest variation across individuals, or (3) focusing sampling on specific areas of interest, e.g., by using spatial redundancy as a vehicle to increase measurement robustness. Algorithms can be designed to iteratively sub-sample sites across configurations with the general aim of finding sampling nodes that adaptively optimize a particular criterion.

A drawback of using interpolating or random field functions to estimate spatial variation is their susceptibility to spatial autocorrelation of measured deformations (e.g., Laslett 1994). On the one hand, autocorrelation of errors may affect the precision of estimates by obscuring actual trends of variation (Laslett 1994); perhaps more problematic, however, is the fact that evaluating continuous interpolation functions at discrete locations tends to produce patterns of interpolated values that are more influenced by landmarks in their immediate vicinity. If a user chooses to minimize the number of landmarks, for example to speed the sampling process, the quality of the interpolated information will suffer. As shown in simulations (see Fig. 7), this issue can be mitigated by increasing the density of sampled landmarks and semi-landmarks prior to interpolation, thus decreasing the weight of individual landmarks on interpolated values in their immediate surroundings. The use of interpolation-based analyses may thus alter the tradeoff between how well a form is sampled, and how many individuals can be sampled.

Landmarks and Jacobians Capture Different Aspects of Local Shape Variation

Even though most users of geometric morphometric methods would reject treating individual landmark coordinates as meaningful univariate variables, subsets of landmarks are typically considered appropriate objects to capture local shape information. Access to local information, in turn, is crucial to answer many biologically relevant questions. Defining parts in terms of collection of landmarks often implies treating individual coordinates as unstructured (i.e., exchangeable) random variables in multivariate analyses, thus losing spatial information necessary to ascertain their specific contribution to shape. Such loss of spatial information is not limited to specific subsets, because adjacent subsets and, in fact, whole configurations may affect local information such that it can become impossible to accurately interpret deformations without fully taking into account their spatial context.

Our results demonstrate that landmark partitions contain insufficient information to infer the shape transformations of the morphological regions that they presumably sample. The choice of whether one uses the simultaneously aligned data or the realigned partitions (Klingenberg 2009) merely alters the specific aspects of shape variation that are lost. Simultaneous alignment preserves deformation patterns defined in the context of whole pre-shapes, therefore accurately localizing focal deformations for the purpose of visual representation. At the same time it confounds local and global sources of variation, implying that simultaneously aligned partitions tend to overestimate shape variation (Klingenberg 2009). This is particularly visible in regions with nearly invariant shape that are adjacent to highly variable ones (see Fig. 4). In contrast, separately aligned partitions accurately estimate focal variances by mapping each partition to its own shape space. Such realignment, however, could lead to a systematic misrepresentation of the shape of partitions by ignoring their context and redistributing landmark variation during Least Squares fit (e.g., van der Linde and Houle 2009). All of these issues derive from the fact that shape is a property of whole configurations that cannot, in general, be allocated to arbitrary focal points without distortion or loss of information. Furthermore, as shown in the study of rodent mandibles, artificial segmentation of otherwise integrated information may not only lead to misconstruing local shape changes, but also to a loss of statistical power.

A Role for Explicit Models in Geometric Morphometrics

Using explicit modeling as a core measurement and estimation approach in geometric morphometrics is, we argue, an unavoidable consequence of using landmarks to infer shape. All geometric morphometric analysis entails assumptions about the ergodicity of landmark configurations, i.e., whether information at a landmark predicts variation at inter-landmark regions. Use of explicit models adds a novel layer of decision-making to geometric

morphometrics for which there are few guidelines at present. The interpolation function used in previous examples, TPS, has been chosen not because of empirical or theoretical support of any kind, but due to their mathematical properties (Bookstein 1992). TPS produces the smoothest possible interpolation, and thus tends to spread local information globally (Rohr 2003; Holden 2008), so that even highly localized deformations tend to influence inferred deformations at regions with little actual landmark data. There are, in fact, a variety of alternatives to TPS modeled after other non-rigid systems (reviewed by Rohr 2003; Holden 2008), such as those based on elastic solids (Davis et al. 1995, 1997), which may prove better suited to model localized deformations in biological forms.

Model choice is rarely a straightforward affair but available approaches, i.e., least squares, Bayesian, maximum likelihood, and information-based methods, could in principle be adapted to facilitate this choice in geometric applications (cf. Grenander and Miller 1998). It is clear that models should be treated as falsifiable hypotheses of shape deformation.

Prospects—A large number of biological questions related to the nature of morphological variation are meaningful only in the context of local variation. We have briefly explored methods appropriate for addressing some of these questions, such as testing for associations between genomic variation and local morphological variation, or comparing variation patterns to a priori hypotheses of morphological integration. These questions, in turn, are key to efforts to link genetic, developmental, and morphological variation, that is to build a genotype-phenotype map (Wagner and Altenberg 1996; Houle 2010), and thus models for the analysis of biological shape should arise from mechanistic, i.e., genetic and developmental, considerations. The search for models that can explain phenotypic variation is a problem with a much wider appeal. For instance, these efforts constitute the basis for a number of disciplines, such as computational morphodynamics (Chen and Brodland 2008; Roeder et al. 2011), which combine visualization techniques and mathematical modeling to understand the mechanisms at gene and cellular levels that underlie the development of macroscopic structures (e.g., Farhadifar et al. 2007; Blanchard et al. 2009; Aegerter-Wilmsen et al. 2010). Development of model-based geometric morphometrics may be able to link the “languages” of functional genomics, developmental mechanics, and phenotypic variation.

It remains to be explored whether available interpolation functions, such as TPS and related radial basis functions, provide promising avenues for the incorporation or consolidation of biologically relevant models into shape analysis. These functions are based on mechanical deformation models that represent the behavior of particular materials under pressure or stress (Holden 2008). The resulting deformations are thus metaphors, and hence potentially problematic when used as models of biological variation. The fact that many of the experimentally-based attempts to link development and form mathematically are based on biomechanical and mechanochemical properties of viscoelastic fields undergoing stress (reviewed by Humphrey 2003; Davidson et al. 2009; Roeder et al. 2011), suggests ample common ground to pursue unitary models to explain both patterns and mechanisms underlying shape variation. Some examples include the organizing role of anisotropic cortical strain distributions on planar cell polarity (e.g., Aigouy et al. 2010), cell and tissue deformation (e.g., Rauzi et al. 2008; Blanchard et al. 2009; Rauzi and Lenne 2011), growth (e.g., Nelson et al. 2005; Shraiman 2005), and epithelial packing (Farhadifar et al. 2007; Aegerter-Wilmsen et al. 2010). Models derived from these processes could increase the accuracy of interpolated estimates of local shape and be tested for empirical support at a macroscopic level.

Acknowledgments

This work was funded by the National Institutes of Health through the NIH Roadmap for Medical Research, Grant U54 RR021813 and through National Science Foundation grant DEB-0950002. Information on the National Centers for Biomedical Computing can be obtained from http://nihroadmap.nih.gov/bioinformatics. We thank Thomas Hansen for his valuable insights on uses of interpolation methods, and J. Kent and three anonymous reviewers for insightful comments. Analyses and simulations were based on code written on SAS, Matlab, Java, C++, and Python. Code used for simulations and in the computation of Jacobians for Drosophila wing data is available upon request from E.M. and R.C., respectively. In addition, a user-friendly Matlab-based standalone package to carry out most of the analyses and to generate all of the graphic outputs shown in this paper has been made available at http://bio.fsu.edu/~dhoule/Software/.

References

Ackermann RR. Morphological integration and the interpretation of fossil hominin diversity. Evolutionary Biology. 2009; 36:149–156.

Aegerter-Wilmsen T, Smith AC, Christen AJ, Aegerter CM, Hafen E, Basler K. Exploring the effects of mechanical feedback on epithelial topology. Development. 2010; 137:499–506. [PubMed: 20081194]

Aigouy B, Farhadifar R, Staple DB, Sagner A, Röper JC, Jülicher F, et al. Cell flow reorients the axis of planar polarity in the wing epithelium of *Drosophila*. Cell. 2010; 142:773–786. [PubMed: 20813263]

Albert AYK, Sawaya S, Vines TH, Knecht AK, Miller CT, Summers BR, et al. The genetics of adaptive shape shift in stickleback: Pleiotropy and effect size. Evolution. 2008; 61:76–85. [PubMed: 18005154]

Atchley WR, Cowley DE, Vogl C, McLellan T. Evolutionary divergence, shape change, and genetic correlation structure in the rodent mandible. Systematic Biology. 1992; 41:196–221.

Atchley WR, Hall BK. A model for development and evolution of complex morphological structures. Biological Reviews of the Cambridge Philosophical Society. 1991; 66:101–157. [PubMed: 1863686]

Ayroles JF, Carbone MA, Stone EA, Jordan KW, Lyman RF, Magwire MM, et al. Systems genetics of complex traits in *Drosophila melanogaster*. Nature Genetics. 2009; 41:299–307. [PubMed: 19234471]

Baylor College of Medicine/Human Genome Sequencing Center. Drosophila Genetic Reference Panel lines at Human Genome Sequencing Center. 2010. http://www.hgsc.bcm.tmc.edu/project-species-i-DGRP_lines.hgsc. Cited 7 July 2011

Blanchard GB, Kabla AJ, Schultz NL, Butler LC, Sanson B, Gorfinkiel N, et al. Tissue tectonics: Morphogenetic strain rates, cell shape change and intercalation. Nature Methods. 2009; 6:458–464. [PubMed: 19412170]

Bookstein FL. Size and shape spaces for landmark data in two dimensions. Statistical Science. 1986; 1:181–242.

Bookstein, FL. Morphometric tools for landmark data: Geometry and biology. Cambridge: Cambridge University Press; 1992.

Boyer DM, Lipman Y, St Clair E, Puente J, Patel BA, Funkhouser T, Jernvall J, Daubechies I. Algorithms to automatically quantify the geometric similarity of anatomical surfaces. Proceedings of National Academy of Science USA. 2011; 108:18221–18226.

Burgio G, Baylac M, Heyer E, Montagutelli X. Genetic analysis of skull shape variation and morphological integration in the mouse using interspecific recombinant congenic strains between C57Bl/6 and mice of the *Mus spretus* species. Evolution. 2009; 63:2668–2686. [PubMed: 19490077]

Cardini A. The geometry of the marmot (Rodentia: Sciuridae) mandible: Phylogeny and patterns of morphological evolution. Systematic Biology. 2003; 52:186–205. [PubMed: 12746146]

Catalano SA, Goloboff PA, Giannini NP. Phylogenetic morphometrics (I): The use of landmark data in a phylogenetic framework. Cladistics. 2010; 26:539–549.

Caumul R, Polly PD. Phylogenetic and environmental components of morphological variation: Skull, mandible, and molar shape in marmots (Marmota, Rodentia). Evolution. 2005; 59:2460–2472. [PubMed: 16396186]

Chen X, Brodland GW. Multi-scale finite element modeling allows the mechanics of amphibian neurulation to be elucidated. Physics and Biology. 2008; 5:15003.

Cheverud JM, Hartman SE, Richtsmeier JT, Atchley WR. A quantitative genetic analysis of localized morphology in mandibles of inbred mice using finite element scaling analysis. Journal of Craniofacial Genetics and Developmental Biology. 1991; 11:122–137. [PubMed: 1761645]

Cheverud JM, Lewis JL, Bachrach W, Lew WD. The measurement of form and variation in form: An application of 3-dimensional quantitative morphology by finite-element methods. American Journal of Physical Anthropology. 1983; 62:151–165. [PubMed: 6650677]

Cheverud JM, Richtsmeier JT. Finite-element scaling applied to sexual dimorphism in rhesus macaques (*Macaca mulatta*) facial growth. Systematic Zoology. 1986; 35:381–399.

Cheverud JM, Wagner GP, Dow MM. Methods for the comparative analysis of variation patterns. Systematic Biology. 1989; 38:201–213.

Commonwick O, Stefanescu R, Fillard P, Arsigny V, Ayache N, Pennec X, et al. Incorporating statistical measures of anatomical variability in atlas-to-subject registration for conformal brain radiotherapy. Medical Image Computing and Computer-Assisted Intervention. 2005; 8:927–934. [PubMed: 16686049]

Cressie, NAC. Statistics for spatial data. Chichester: Wiley; 1993.

Davidson M, von Dassow M, Zhou J. Multi-scale mechanics from molecules to morphogenesis. International Journal of Biochemistry and Cell Biology. 2009; 41:2147–2162. [PubMed: 19394436]

Davis, MH.; Khotanzad, A.; Flamig, DP.; Harms, SE. Elastic body splines: A physics-based approach to coordinate transformation in medical image matching. Proceedings of 8th IEEE Symposium on Computer and Medical Systems; 1995. p. 81-88.

Davis MH, Khotanzad A, Flamig DP, Harms SE. A physics-based coordinate transformation for 3-D image matching. IEEE Transactions on Medical Imaging. 1997; 16:317–328. [PubMed: 9184894]

Dryden, IL.; Mardia, KV. Statistical shape analysis. Chichester: Wiley; 1998.

Dworkin I, Gibson G. Epidermal growth factor receptor and transforming growth factor-beta signaling contributes to variation for wing shape in *Drosophila melanogaster*. Genetics. 2006; 173:1417–1431. [PubMed: 16648592]

Dworkin I, Palsson A, Gibson G. Replication of an *Egfr*-wing shape association in a wild-caught cohort of *Drosophila melanogaster*. Genetics. 2005; 169:2115–2125. [PubMed: 15687273]

Escoufier Y. Le traitement des variables vectorielles. Biometrics. 1973; 29:751–760.

Farhadifar R, Roper JC, Algouy B, Eaton S, Julicher F. The influence of cell mechanics, cell–cell interactions, and proliferation on epithelial packing. Current Biology. 2007; 17:2095–2104. [PubMed: 18082406]

Feng X, Wilson Y, Bowers J, Kennaway R, Bangham A, Hannah A, et al. Evolution of allometry in *Antirrhinum*. The Plant Cell. 2009; 21:2999–3007. [PubMed: 19880796]

González-José R, Escapa I, Neves WA, Cúneo R, Pucciarelli HM. Cladistic analysis of continuous modularized traits provides phylogenetic signals in *Homo* evolution. Nature. 2008; 453:775–778. [PubMed: 18454137]

Goovaerts, P. Geostatistics for natural resources evaluation. New York: Oxford University Press; 1997.

Grenander U, Miller MI. Computational anatomy: An emerging discipline. Quarterly of Applied Mathematics. 1998; 56:617–694.

Haley CS, Knott SA. A simple regression method for mapping quantitative trait loci in line crosses using flanking markers. Heredity. 1992; 69:315–324. [PubMed: 16718932]

Hall BK, Miyake T. All for one and one for all: Condensations and the initiation of skeletal development. Bioessays. 2000; 22:138–147. [PubMed: 10655033]

Hallgrímsson B, Jamniczky HA, Young NM, Rolian C, Parsons TE, Boughner JC, et al. Deciphering the Palimpsest: Studying the relationship between morphological integration and phenotypic covariation. Evolutionary Biology. 2009; 36:355–376.

Hine E, Blows MW. Determining the effective dimensionality of the genetic variance-covariance matrix. Genetics. 2006; 173:1135–1144. [PubMed: 16547106]

Holden M. A review of geometric transformations for nonrigid body registration. IEEE Transactions on Medical Imaging. 2008; 27:111–128. [PubMed: 18270067]

Houle D. Numbering the hairs on our heads: The shared challenge and promise of phenomics. Proceedings of National Academy of Science USA. 2010; 107:1793–1799.

Humphrey JD. Continuum biomechanics of soft biological tissues. Proceedings of the Royal Society (Part A): Mathematical, Physical, and Engineering Sciences. 2003; 459:3–46.

Hutchinson MF, Gessler PE. Splines—More than just a smooth interpolator. Geoderma. 1994; 62:45–67.

Klingenberg CP. Morphological integration and developmental modularity. Annual Review of Ecology and Systematics. 2008; 39:115–132.

Klingenberg CP. Morphometric integration and modularity in configurations of landmarks: Tools for evaluating a priori hypotheses. Evolution & Development. 2009; 11:405–421. [PubMed: 19601974]

Klingenberg CP. Evolution and development of shape: Integrating quantitative approaches. Nature Review. 2010; 11:623–635.

Klingenberg CP, Gidaszweski NA. Testing and quantifying phylogenetic signals and homoplasy in morphometric data. Systematic Biology. 2010; 59:245–261. [PubMed: 20525633]

Klingenberg CP, Leamy LJ, Routman EJ, Cheverud JM. Genetic architecture of mandible shape in mice: Effects of quantitative trait loci analyzed by geometric morphometrics. Genetics. 2001; 157:785–802. [PubMed: 11156997]

Klingenberg CP, Mebus K, Auffray JC. Developmental integration in a complex morphological structure: How distinct are the modules in the mouse mandible? Evolution & Development. 2003; 5:522–531. [PubMed: 12950630]

Laslett GM. Kriging and splines: An empirical comparison of their predictive performance in some applications. Journal of the American Statistical Association. 1994; 89:391–400.

Leamy LJ, Klingenberg CP, Sherratt E, Wolf JB, Cheverud JM. A search for quantitative trait loci exhibiting imprinting effects on mouse mandible size and shape. Heredity. 2008; 101:518–526. [PubMed: 18685568]

Leamy LJ, Routman EJ, Cheverud JM. Quantitative trait loci for early- and late-developing skull characters in mice: A test of the genetic independence model of morphological integration. American Naturalist. 1999; 153:201–214.

Lewis JL, Lew WD, Zimmerman JR. A nonhomogeneous anthropometric scaling method based on finite element principles. Journal of Biomechanics. 1980; 13:815–824. [PubMed: 7462255]

MacLeod, N. Phylogenetic signals in morphometric data. In: MacLeod, N.; Forey, PL., editors. Morphology, shape and phylogeny. London: Taylor & Francis; 2002. p. 100-138.

Mardia KV, Kent JT, Goodall CR, Little JA. Kriging and splines with derivative information. Biometrika. 1996; 83:207–221.

Márquez EJ. A statistical framework for testing modularity in multidimensional data. Evolution. 2008; 62:2688–2708. [PubMed: 18691262]

Márquez EJ, Knowles LL. Correlated evolution of multivariate traits: Detecting co-divergence across multiple dimensions. Journal of Evolutionary Biology. 2007; 20:2334–2348. [PubMed: 17956395]

Marroig G, Cheverud JM. A comparison of phenotypic variation and covariation patterns and the role of phylogeny, ecology and ontogeny during cranial evolution of New World Monkeys. Evolution. 2001; 55:2576–2600. [PubMed: 11831671]

Martínez-Abadías N, Paschetta C, de Azevedo S, Esparza M, González-José R. Developmental and genetic constraints on neurocranial globularity: Insights from analyses of deformed skulls and quantitative genetics. Evolutionary Biology. 2009; 36:37–56.

Matheron G. The intrinsic random functions and their applications. Advances in Applied Probability. 1973; 5:439–468.

McAlarney ME. Use of the boundary element method for biological morphometrics. Journal of Biomechanics. 1995; 28:609–616. [PubMed: 7775496]

McAlarney ME, Chiu WK. Comparison of numeric techniques in the analysis of cleft palate dental arch form change. The Cleft Palate-Craniofacial Journal. 1997; 34:281–291. [PubMed: 9257018]

McGuigan K, Blows MW. Evolvability of individual traits in a multivariate context: Partitioning the additive genetic variance into common and specific components. Evolution. 2010; 64:1899–1911. [PubMed: 20148952]

Meinguet J. Multivariate interpolation at arbitrary points made simple. Journal of Applied Mathematics and Physics. 1979; 30:292–304.

Mezey JG, Cheverud JM, Wagner GP. Is the genotype-phenotype map modular?: A statistical approach using mouse quantitative trait loci data. Genetics. 2000; 156:305–311. [PubMed: 10978294]

Mezey JG, Houle D. The dimensionality of genetic variation for wing shape in *Drosophila melanogaster*. Evolution. 2005; 59:1027–1038. [PubMed: 16136802]

Mezey JG, Houle D, Nuzhdin SV. Naturally segregating quantitative trait loci affecting wing shape of *Drosophila melanogaster*. Genetics. 2005; 169:2101–2113. [PubMed: 15520257]

Mitteroecker P, Bookstein F. The conceptual and statistical relationship between modularity and morphological integration. Systematic Biology. 2007; 56:818–836. [PubMed: 17934997]

Monteiro LR, Bonato V, dos Reis SF. Evolutionary integration and morphological diversification in complex morphological structures: Mandible shape divergence in spiny rats (Rodentia, Echimyidae). Evolution & Development. 2005; 7:429–439. [PubMed: 16174036]

Monteiro LR, Nogueira MR. Adaptive radiations, ecological specialization, and the evolutionary integration of complex morphological structures. Evolution. 2010; 64:724–743. [PubMed: 19804403]

Moss ML, Vilmann H, Moss-Salentjin L, Sen K, Pucciarelli HM, Skalak R. Studies on orthocephalization: Growth behavior of the rat skull in the period 13–49 days as described by the finite element method. American Journal of Physical Anthropology. 1987; 72:323–342. [PubMed: 3578496]

Nelson CM, Jean RP, Tan JL, Liu WF, Sniadecki NJ, Spector AA, et al. Emergent patterns of growth controlled by multicellular form and mechanics. Proceeding of National Academy of Science, USA. 2005; 102:11594–11599.

Pepper, DW.; Heinrich, JC. The finite element method: Basic concepts and applications. New York: Hemisphere Pub Co; 1992.

Rauzi M, Lenne PF. Cortical forces in cell shape changes and tissue morphogenesis. Current Topics in Developmental Biolology. 2011; 95:93–144.

Rauzi M, Verant P, Lecuit T, Lenne PF. Nature and anisotropy of cortical forces orienting *Drosophila* tissue morphogenesis. Nature Cell Biology. 2008; 10:1401–1410.

Richstmeier JT, DeLeon VB. Morphological integration of the skull in craniofacial anomalies. Orthodontics and Craniofacial Research. 2009; 12:149–158. [PubMed: 19627516]

Richtsmeier, JT.; Lele, SR.; Cole, TM, III. Landmark morphometrics and the analysis of variation. In: Hallgrímsson, B.; Hall, BK., editors. Variation: A central concept in biology. Burlington: Academic Press; 2005. p. 49-69.

Roeder AHK, Tarr PT, Tobin C, Zhang X, Chickarmane V, Cunha A, et al. Computational morphodynamics of plants: Integrating development over space and time. Nature Reviews Molecular Cell Biology. 2011; 12:265–273.

Rohlf FJ. Shape statistics: Procrustes superimpositions and tangent spaces. Journal of Classification. 1999; 16:197–223.

Rohr, K. Landmark-based image analysis: Using geometric and intensity models. Dordrecth: Kluwer; 2001.

Rohr K. Spline-based elastic image registration. Proceedings in Applied Mathematics and Mechanics. 2003; 3:36–39.

Rohr K, Stiehl HS, Sprengel R, Buzug TM, Weese J, Kuhn MH. Landmark-based elastic registration using approximating thin-plate splines. IEEE Transactions on Medical Imaging. 2001; 20:526–534. [PubMed: 11437112]

Schabenberger, O.; Gotway, CA. Statistical methods for spatial data analysis. Boca Raton: CRC Press; 2005.

Shraiman BI. Mechanical feedback as a possible regulator of tissue growth. Proceedings of the National Academy of Science USA. 2005; 102:3318–3323.

Stelkens RB, Schmid C, Selz O, Seehausen O. Phenotypic novelty in experimental hybrids is predicted by the genetic distance between species of cichlid fish. BMC Evolutionary Biology. 2009; 9:283. [PubMed: 19961584]

van der Linde K, Houle D. Inferring the nature of allometry from geometric data. Evolutionary Biology. 2009; 36:311–322.

Wagner GP. A comparative study of morphological integration in *Apis mellifera* (Insecta, Hymenoptera). Journal of Zoological Systematics and Evolutionary Research. 1990; 28:48–61.

Wagner GP, Altenberg L. Complex adaptations and the evolution of evolvability. Evolution. 1996; 50:967–976.

Wahba, G. Spline models for observational data. CBMS-NSF Regional Conference Series in Applied Mathematics; 1990.

Walker JA. Ability of geometric morphometric methods to estimate a known covariance matrix. Systematic Biology. 2000; 49:686–696. [PubMed: 12116434]

Woods RP. Characterizing volume and surface deformations in an atlas framework: Theory, applications, and implementation. NeuroImage. 2003; 18:769–788. [PubMed: 12667854]

Workman MS, Leamy LJ, Routman EJ, Cheverud JM. Analysis of quantitative trait locus effects on the size and shape of mandibular molars in mice. Genetics. 2002; 160:1573–1586. [PubMed: 11973311]

Yang J, Lee SH, Goddard ME, Visscher PM. GCTA: A tool for genome-wide complex trait analysis. American Journal of Human Genetics. 2011; 88:76–82. [PubMed: 21167468]

Young RL, Badyaev A. Evolutionary persistence of phenotypic integration: Influence of developmental and functional relationships on complex traits evolution. Evolution. 2006; 60:1291–1299. [PubMed: 16892978]

Zelditch, ML.; Swiderski, DL.; Sheets, HD.; Fink, WL. Geometric morphometrics for biologists: A primer. San Diego: Elsevier; 2004.

Zelditch ML, Wood AR, Bonett RM, Swiderski DL. Modularity of the rodent mandible: Integrating bones, muscles, and teeth. Evolution & Development. 2008; 10:756–768. [PubMed: 19021747]

Zelditch ML, Wood AR, Swiderski DL. Building developmental integration into functional systems: Function-induced integration of mandibular shape. Evolutionary Biology. 2009; 36:71–87.

Zienkiewicz, OC. The finite element method in engineering science. London: McGraw-Hill; 1971.

Zimmerman E, Palsson A, Gibson G. Quantitative trait loci affecting components of wing shape in *Drosophila melanogaster*. Genetics. 2000; 155:671–683. [PubMed: 10835390]

Appendix

The following sections provide mathematical details for the interpolation approaches discussed in this work, emphasizing common principles shared by these methods.

Interpolating Splines

Interpolating spline functions use information contained in landmark-wise differences between two configurations to map every location in a reference configuration onto a target form (Woods 2003). In general, m-dimensional interpolant functions are optimized by minimizing a roughness penalty $\rho \in \mathbb{R}^m$ ($m = 1, 2, 3$), defined in terms of the second order partial derivatives of the interpolant function $\mathbf{\Phi}(\mathbf{p})$

$$\rho(\Phi_{x,y})=\int\int_{R^2}\left(\frac{\partial^2\Phi}{\partial x^2}\right)^2+\left(\frac{\partial^2\Phi}{\partial y^2}\right)^2+2\left(\frac{\partial^2\Phi}{\partial x\partial y}\right)^2 \mathrm{d}x\mathrm{d}y \quad (3)$$

for the 2-D case (Dryden and Mardia 1998), and

$$\rho(\Phi_{x,y,z})=\int\int\int_{R^3}\left(\frac{\partial^2\Phi}{\partial x^2}\right)^2+\left(\frac{\partial^2\Phi}{\partial y^2}\right)^2+\left(\frac{\partial^2\Phi}{\partial z^2}\right)^2+2\left(\frac{\partial^2\Phi}{\partial x\partial y}\right)^2+2\left(\frac{\partial^2\Phi}{\partial x\partial z}\right)^2+2\left(\frac{\partial^2\Phi}{\partial y\partial z}\right)^2 \mathrm{d}x\mathrm{d}y\mathrm{d}z \quad (4)$$

for the 3-D case (Meinguet 1979). The minimized sum of $\rho(\Phi)$ over splines is the minimum penalty incurred from deforming a set of fixed set of landmarks into another set of equivalent (e.g., homologous) landmarks (Bookstein 1992), and it is termed the total bending energy. Minimization of Eqns. 3 and 4 leads to the smooth interpolation of deformation values at arbitrary locations of the form.

The interpolating splines emphasized in this study, namely TPS, belongs to a class of interpolants termed radial basis functions (RBF; Rohr 2001; Holden 2008), with general form

$$\Phi(\mathbf{p})=\sum_j^h \beta_j U_j(\mathbf{p})+\sum_i^k \alpha_i R(\left\|\mathbf{p}-\mathbf{q}_i\right\|) \quad (5)$$

where $\Phi(\mathbf{p})$ represents the interpolation function at the 2- or 3-D point **p** (Holden 2008). In this formalism, a deformation is modeled as the sum of an affine component, given by $U(\mathbf{p})$, and a function R that provides the non-affine component of the deformation, which smoothes the propagation of deformations throughout an object as a function of the distance between the interpolation point **p** and sampled landmarks $\mathbf{q}_i$ ($i = 1, \ldots, k$). Thus, the influence of a landmark on the non-affine component of an interpolated site decays with the distance between the two locations, i.e., $\|\mathbf{p} - \mathbf{q}_i\|$. Finally, β_j and α_i are weights for the affine and non-affine components, respectively. Eqns. 3 and 4 can be solved as a set of linear equations with general form:

$$\begin{bmatrix} \mathbf{R} & \mathbf{Q} \\ \mathbf{Q} & 0 \end{bmatrix}\begin{bmatrix} \alpha \\ \beta \end{bmatrix}=\begin{bmatrix} \mathbf{P} \\ 0 \end{bmatrix} \quad (6)$$

which describes a deformation of a reference configuration **Q** onto a known target configuration **P** (Holden 2008). Deformation functions $R_i = R(\|\mathbf{p} - \mathbf{q}_i\|)$ are collected in matrix **R**, and we solve for vectors of coefficients $\boldsymbol{\alpha}$ and $\boldsymbol{\beta}$.

A set of thin-plate splines is given by the function

$$[\Phi_1(\mathbf{p}),\ldots,\Phi_m(\mathbf{p})]^T=\mathbf{b}+\mathbf{A}\mathbf{p}+\mathbf{W}^T r(\mathbf{p}) \quad (7)$$

where **b** + **Ap** defines the affine component of the deformation, **b** ($m \times 1$), **A** ($m \times m$), and **W** ($k \times m$) are represented by coefficients α and β in Eqns. 5 and 6, and $r(\mathbf{p}) = (R(\mathbf{p} - \mathbf{q}_1), \ldots, R(\mathbf{p} - \mathbf{q}_k))^T$ is computed using the logarithmic interpolants $R_i=r_i^2\log r_i$ (for 2-D) and $R_i =$ (for 3-D), where r_i represent the Euclidean distances between each landmark and the interpolation point in the reference (Bookstein 1992; Dryden and Mardia 1998). Unknown coefficients in Eqn. 7 are estimated using the set of linear equations

$$\begin{bmatrix} \mathbf{R} & \mathbf{1}_k & \mathbf{Q} \\ \mathbf{1}_k^T & 0 & 0 \\ \mathbf{Q}^T & 0 & 0 \end{bmatrix} \begin{bmatrix} \mathbf{W} \\ \mathbf{b}^T \\ \mathbf{A}^T \end{bmatrix} = \begin{bmatrix} \mathbf{P} \\ 0 \\ 0 \end{bmatrix} \quad (8)$$

where R_{ij} elements from **R** ($k \times k$) are computed using the interpolation function between all possible pairs of landmarks in the reference (using $R_{ij} = 0$ for $i = j$), $\mathbf{1}_k$ ($k \times 1$) is a vector of ones, and **Q** and **P** ($k \times m$) are the reference and target configurations being compared, respectively (Dryden and Mardia 1998).

Smoothing Splines

One generalization of the spline methodology treats the choice and adjustment of interpolant functions as an estimation problem, where landmarks are assumed to be measured with error that is minimized prior to computation of the splines (Hutchinson and Gessler 1994). In this approach, sampled landmarks **q** are modeled as instances of an intrinsic function $g(\mathbf{q})$, so that $q_i = g(q_i) + \varepsilon_i(q_i)$, where ε_i denotes an error function (Hutchinson and Gessler 1994; Laslett 1994). The idea is to choose the function g that best predicts the values at sampled landmarks (Laslett 1994). The optimal function is the one that minimizes the quantity

$$\sum_{i=1}^{n} [q_i - g(q_i)]^2 + \lambda \rho(g(\mathbf{q}))$$

where $\lambda > 0$ is a smoothing parameter, estimable through cross-validation (Wahba 1990; Hutchinson and Gessler 1994), and ρ is as defined in Eqns. 3 and 4, so that $\lambda\rho$ can be treated as a roughness penalty (Dryden and Mardia 1998). When TPS are used as the g function, the system in Eqn. 8 becomes

$$\begin{bmatrix} \mathbf{R} + \lambda \mathbf{I}_k & \mathbf{1}_k & \mathbf{Q} \\ \mathbf{1}_k^T & 0 & 0 \\ \mathbf{Q}^T & 0 & 0 \end{bmatrix} \begin{bmatrix} \mathbf{W} \\ \mathbf{b}^T \\ \mathbf{A}^T \end{bmatrix} = \begin{bmatrix} \mathbf{P} \\ 0 \\ 0 \end{bmatrix} \quad (9)$$

which also can be used for interpolation. Smoothing splines could be used to test among alternative spatial patterns of roughness penalties (λ) given an interpolation function, as well as for choosing among alternative g functions. Simulations have shown, however, that the use of cross-validation to optimally fit splines for spatial prediction often leads to over-smoothing and a consequent loss of valuable spatial information, an issue that seems related to fluctuations in the spatial density of the samples used for interpolation (Laslett 1994).

Kriging

Kriging is a method for linear prediction of the value of a variable using the information contained in a set of neighboring samples (Laslett 1994). Kriging presupposes the existence of a random field $\{Z(\mathbf{p}): \mathbf{p} \in D \subset \mathbb{R}^m\}$ spanning a continuous domain D and observed at sampled points **q**, which determines the value of the variable of interest at each location (Matheron 1973; Schaben-berger and Gotway 2005). The value at any arbitrary site **p** is given by the linear predictor $\hat{Z}(\mathbf{p})$, defined by

$$\widehat{Z}(\mathbf{p})=\sum_{i=1}^{k}\lambda_i Z(\mathbf{q}_i)=\Lambda Z(\mathbf{q})$$

where $\Lambda = [\lambda_1, \ldots, \lambda_k]$ for k landmarks, and λ_i are weights for the **q** landmarks, which are computed based on the information content at each landmark about the true value of the random field at the estimation site $Z(\mathbf{p})$ (Goovaerts 1997). The goal of kriging is to find the weights λ_i that minimize the mean square prediction error $\mathrm{MSPE}(\mathbf{p}) = E[Z(\mathbf{p}) - \hat{Z}(\mathbf{p})^2]$, under the unbiasedness constraint $E[\hat{Z}(\mathbf{p}) - Z(\mathbf{p}) = 0$ (Goovaerts 1997).

The central element of kriging prediction is the covariance function $\sigma(t - s)$, which describes the relationship between the difference between points t and s, and their values in the random field, i.e., $Z(t) - Z(s)$ (Cressie 1993). A common approach in spatial analysis consists of fitting an arbitrary continuous function to an empirical (discrete) variogram and using this function to derive a covariance function (Goovaerts 1997; Cressie 1993). More generally, kriging estimates the covariance function underlying the residual portion $\varepsilon(\mathbf{p})$ of the random field Z given the linear model

$$Z(\mathbf{p})=\sum_{j=1}^{h}\beta_j g_j(\mathbf{p})+\sum_{i=1}^{k}\alpha_i K(\left\|\mathbf{p}-\mathbf{q}_i\right\|) \quad (10)$$

where $\sum_{i=1}^{k}\alpha_i K(\mathbf{p}_i)=\varepsilon(\mathbf{p})$ defines the *residual* and $\sum_{i=1}^{h}\beta_i g_i(\mathbf{p})=E[Z(\mathbf{p})]$ the *trend* of the field, with $g(\mathbf{p}) = [g_1(\mathbf{p}), \ldots, g_h(\mathbf{p})]$ a linear combination of known functions (Matheron 1973; Hutchinson and Gessler 1994). A comparison between Eqns. 5 and 10 suggests similarities between the trend of the random field in kriging and the uniform component of a deformation in terms of splines, and between the unique residuals at each point estimated using kriging with the non-affine component of the interpolating splines. In fact, when the rank of the function monomials $g(\mathbf{p})$ equals the degree of the derivative used to estimate the roughness parameters in splines (see Eqns. 3 and 4) minus one, kriging and interpolating splines are identical methods (Hutchinson and Gessler 1994).

Alternative kriging strategies differ in their treatment of the trend as a universal constant, as a local constant, or as a function, such as an interpolant function, upon which locally predicted mean values are modeled (Goovaerts 1997). The latter, termed universal kriging has been developed in the context of shape deformations by Mardia et al. (1996), whose work has demonstrated that 2-D TPS are in fact universal kriging predictors with covariance function given by $\sigma(r)=r_i^2\log r_i$.

Finite Elements

Finite element methods (FEM) extract local deformation information by generalization or interpolation of the displacement at landmarks forming the vertices of rigid polygons or polyhedrons (Lewis et al. 1980). Two types of FEM have been applied in morphometric studies, namely homogeneous FE, in which shape changes within an element are assumed to be uniform throughout (Bookstein 1986; Moss et al. 1987), and non-homogeneous FE, whereby interpolation is used to model the deformation as a non-linear function of the changes observed at landmarks (Lewis et al. 1980; Cheverud et al. 1983; McAlarney 1995; McAlarney and Chiu 1997).

In homogeneous FEM, a set of normalized landmark displacements of an individual with respect to a reference configuration, A, are used to estimate tensors and principal strains via eigendecomposition of the sum of squares and cross-products matrix $A^T A$ (Bookstein 1986; Moss et al. 1987). The resulting eigenvectors can be envisaged as the principal axes of the ellipse that results from deforming the circumference that passes through all of the vertices of an element in the reference configuration to match the target configuration (Dryden and Mardia 1998). Non-homogeneous FEM, on the other hand, use normalized landmark displacements between reference and target configuration to parameterize a system of continuous functions whose purpose is to find a common set of coefficients that explain both these displacements and all the deformations inside the element boundaries (Lewis et al. 1980). If we denote a shape transformation at the ith vertex of a triangle as $T_i = Q_i + R_i$, (i = 1, 2, 3), where T and Q represent the target and reference configurations, respectively, and R represents a deformation, then for any arbitrary point p within Q, we can write the interpolated value of the deformation at this point as

$$r_p = \sum_{i=1}^{3} \lambda_i R_i \quad (11)$$

(Lewis et al. 1980) where λ denotes vertex-specific weights derived from an interpolation function. In practice, Eqn. 11 can be parameterized using polynomials (Pepper and Heinrich 1992), or an interpolator, such as TPS (Bookstein 1986).

Both types of FEM require a priori choices regarding the shape and location of finite elements, and the absence of unambiguous criteria to make this choice (Cheverud and Richtsmeier 1986) is generally perceived a weakness of the method (McAlarney and Chiu 1997; Dryden and Mardia 1998). In the case of homogeneous FEM, the assumption of spatial uniformity of interpolated values suggests a preference for elements of small size, the optimal choice being to use triangles (2-D) and tetrahedrons (3-D), compiled together as a mesh (Pepper and Heinrich 1992). Even though this choice should lead to relatively precise estimates, it also imposes undesirable restrictions, namely the fact that triangles can only undergo affine deformations (Dryden and Mardia 1998), limiting their usefulness as shape descriptors. Non-homogeneous FEM, on the other hand, can be applied to more complex volumes (e.g., Cheverud et al. 1983), which in turn requires making ad hoc choices regarding which landmarks to use as element vertices, once again incorporating arbitrary elements in the measurement of shape (Zienkiewicz 1971; McAlarney and Chiu 1997; Dryden and Mardia 1998). Additional issues with FEM are the lack of a standard approach for computation of a mean and registration (Cheverud et al. 1983), and the absence of a clear-cut separation of global and local components of a deformation, due to the fact that both components are defined only within elements.

Comparison Among Alternative Methods

The common purpose of shape analysis by interpolation, smoothing, or kriging methods is the estimation or prediction of an unknown local deformation value $Z(\mathbf{p})$ as a function of its spatial location, based on observed landmark deformations, $Z(\mathbf{q})$. Measurements $Z(\mathbf{q})$ are used to infer or parameterize an underlying function $g[Z(\mathbf{p})]$, which is then applied throughout the whole structure under analysis. An analogous function is also derived in non-homogeneous FEM to estimate values within FE.

The function $g[Z(\mathbf{p})]$ comprises two parts: an affine component that captures the portion of the total shape deformation that is shared throughout the whole structure under analysis, and a non-affine component that captures local deviations from the global trend, modeled using

a covariance function tracking the influence of sampled points as a function of the distances amongst them. Splining methods select the function g among the universe of possible functions that minimizes the deformations required to explain the differences between two shapes (Bookstein 1986), according to an a priori deformation model. In kriging, on the other hand, g defines a random field whereby local deformations, whether measured or predicted, are treated as stochastic realizations of an intrinsic process (Matheron 1973). In practical applications, however, the two methods largely overlap (Hutchinson and Gessler 1994).

Thus, interpolation-based shape analyses by smoothing, kriging or finite elements methods are all closely related, and become indistinguishable from interpolating splines under the circumstances we have outlined.

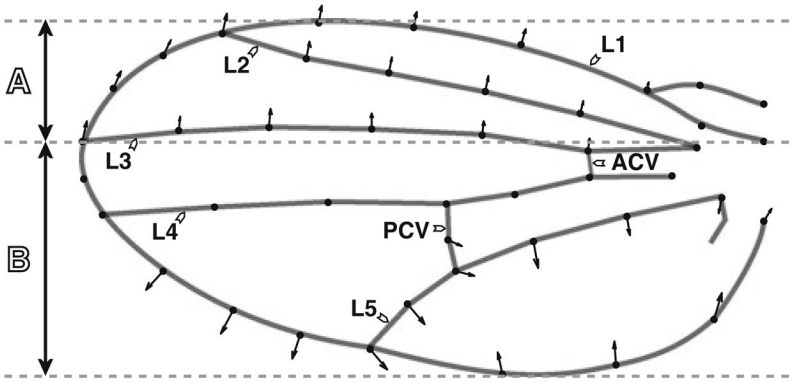

Fig. 1.

Context dependence of shape differences in a hypothetical deformation of the *Drosophila melanogaster* wing. *Arrows* represent landmark differences between a reference, drawn as outlines of wing veins, and a target form. Landmark displacements in the region labeled as **a** suggest substantial correlated differences between target and reference forms, even though the shape they delimit is nearly invariant; landmark displacements in region **b** are of similar magnitudes, yet describe a range of local differences in shape. L1–L5 denote longitudinal veins discussed in text, PCV and ACV denote posterior and anterior cross-veins, respectively

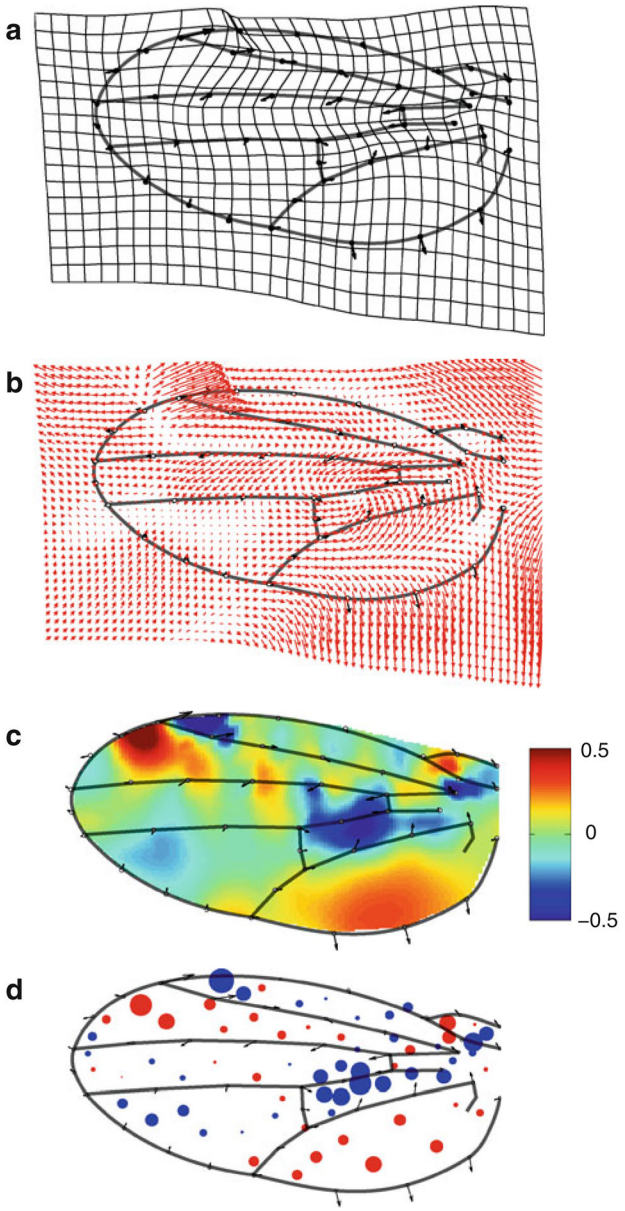

Fig. 2.

Equivalent representations of differences between a target and a reference Drosophila wing interpolated using thin-plate splines. **a** Deformation of a sparse regular grid, the most commonly used deformation representation in geometric morphometric applications; **b** deformation of a dense regular grid represented as a vector field by drawing each node as a velocity vector; **c** heat map representing a scalar field, with pixel tone indicating proportional changes in local (i.e., infinitesimal) area; **d** bubble plot representing a scalar field with bubble diameter proportional to change in local area, where bubble locations correspond to centroids of a triangulated grid anchored on sampled landmarks. Local deformations in **c** and **d** computed as base-2 logarithms of the ratio of local areas of target and reference shapes (e.g., a deformation magnitude of 1 represents a local expansion by a factor of 2, whereas a magnitude of −1 represents a local contraction by a factor of 0.5). These values are estimated as Jacobian determinants of a TPS function

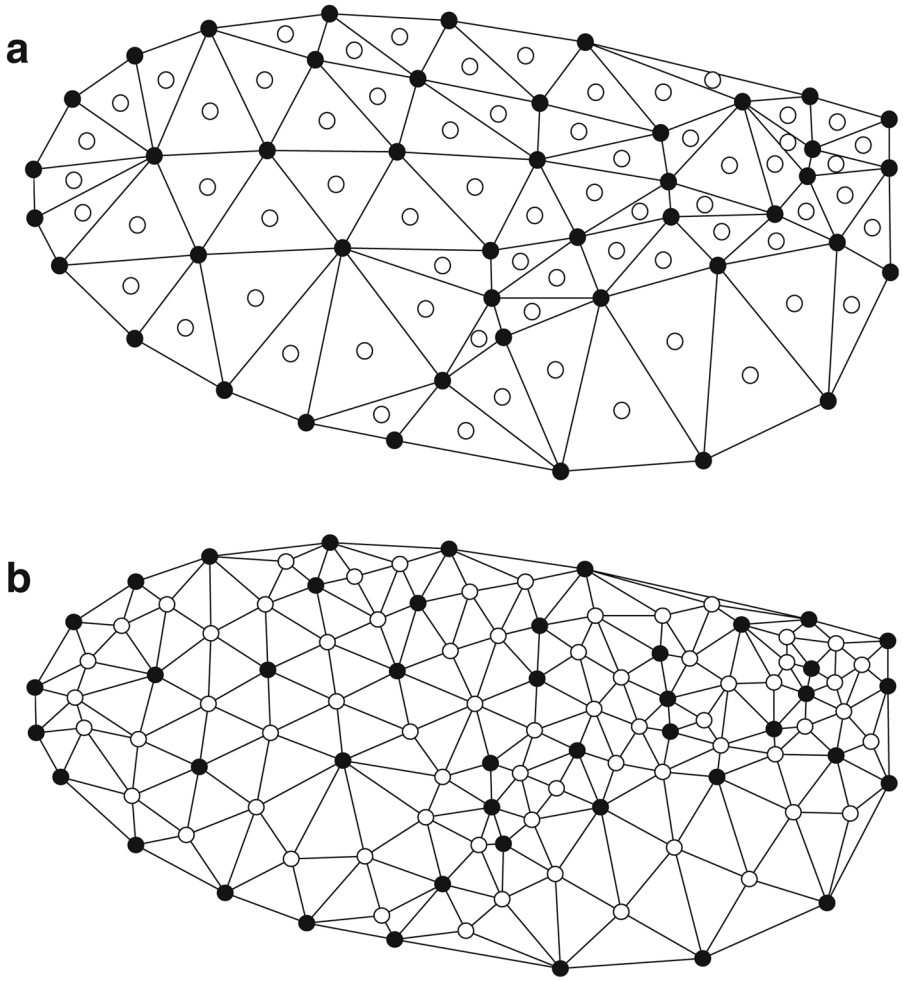

Fig. 3.

Schematic representation of two rounds of Delaunay triangulation in the Drosophila wing data set discussed in the text. **a** Landmarks (*closed circles*) are connected by adjacency rules as defined by the triangulation algorithm, and centroids of the resulting triangles (*open circles*) become evaluation points for interpolation functions; **b** these points can be used along with landmarks in a second round of triangulation, resulting in a denser set of points (triangle centroids not shown)

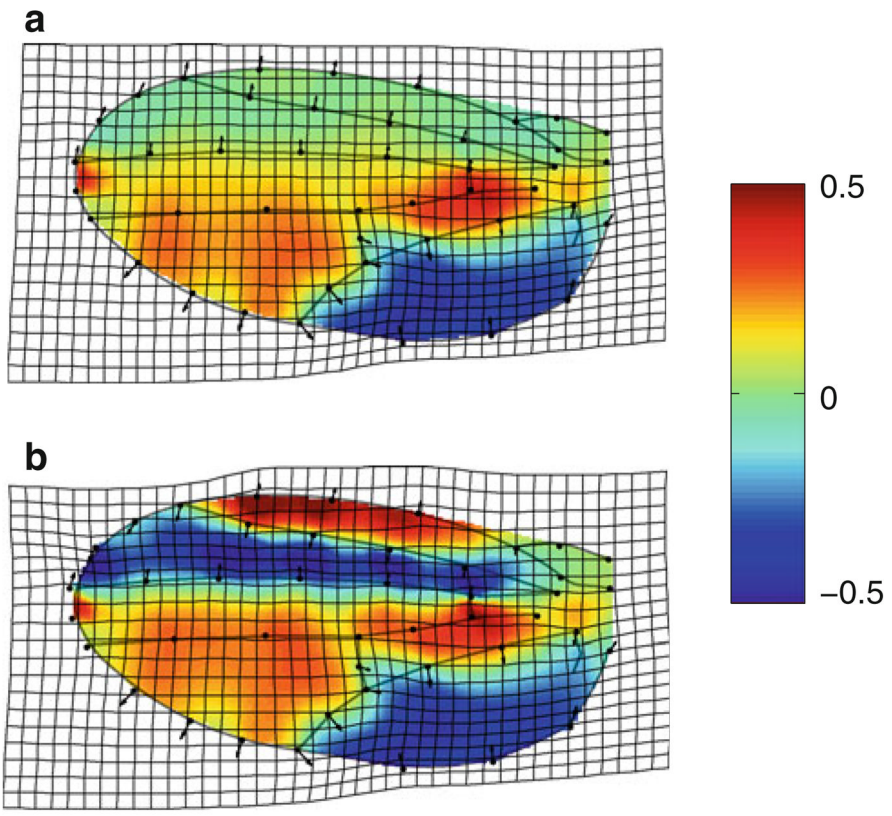

Fig. 4.

Two scenarios used in simulations of patterns of variation of Drosophila wings. Scenario I (**a**) differs from scenario II (**b**) only in the sign of the y-coordinate of the landmark displacements on vein L2. Tones represent base-2 logarithms of the ratio of local areas of target and reference configurations (see text for details). Grid and heat map interpolations are based on TPS functions

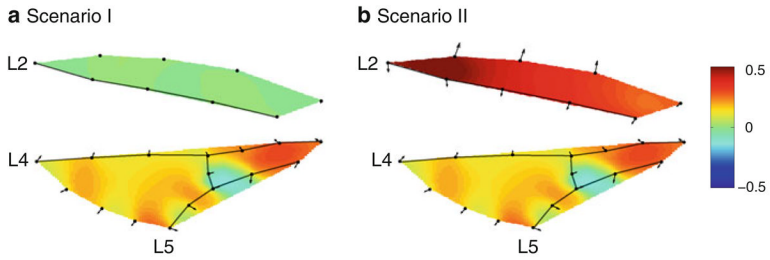

Fig. 5.

Drosophila wing partitions resulting from simulation scenarios depicted in Fig. 4, after been separately aligned. Tones represent proportional magnitudes of deformation in local area (see text for details). Grid and heat map interpolations are based on TPS functions

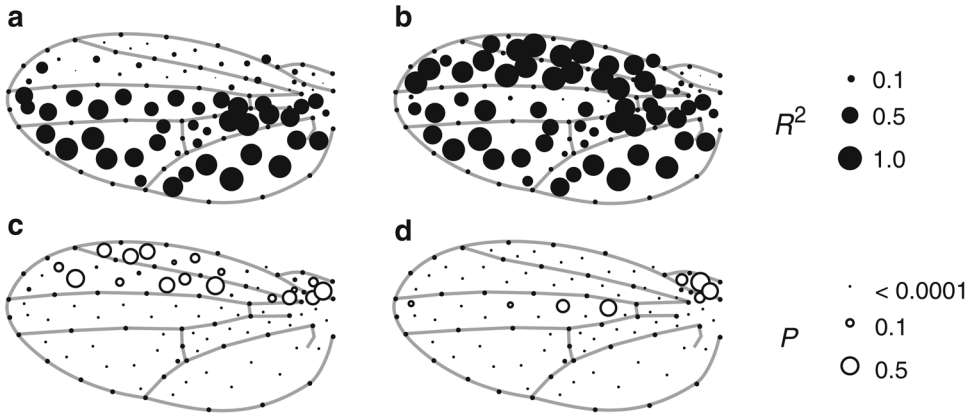

Fig. 6.

Bubble plots representing results from univariate ANOVAs based on estimates of local area change under two simulation scenarios of variation in the Drosophila wing (see Fig. 4 for details). Bubble diameter is proportional to average R^2 (**a**, **b**) and *P* values (**c**, **d**) over 1,000 replicates. Original data consists of base-2 logarithm determinants of Jacobians of a TPS function evaluated on a triangulated grid (see Fig. 2) on each replicated configuration. Original landmarks and semi-landmarks are represented by *closed circles* drawn on wing veins

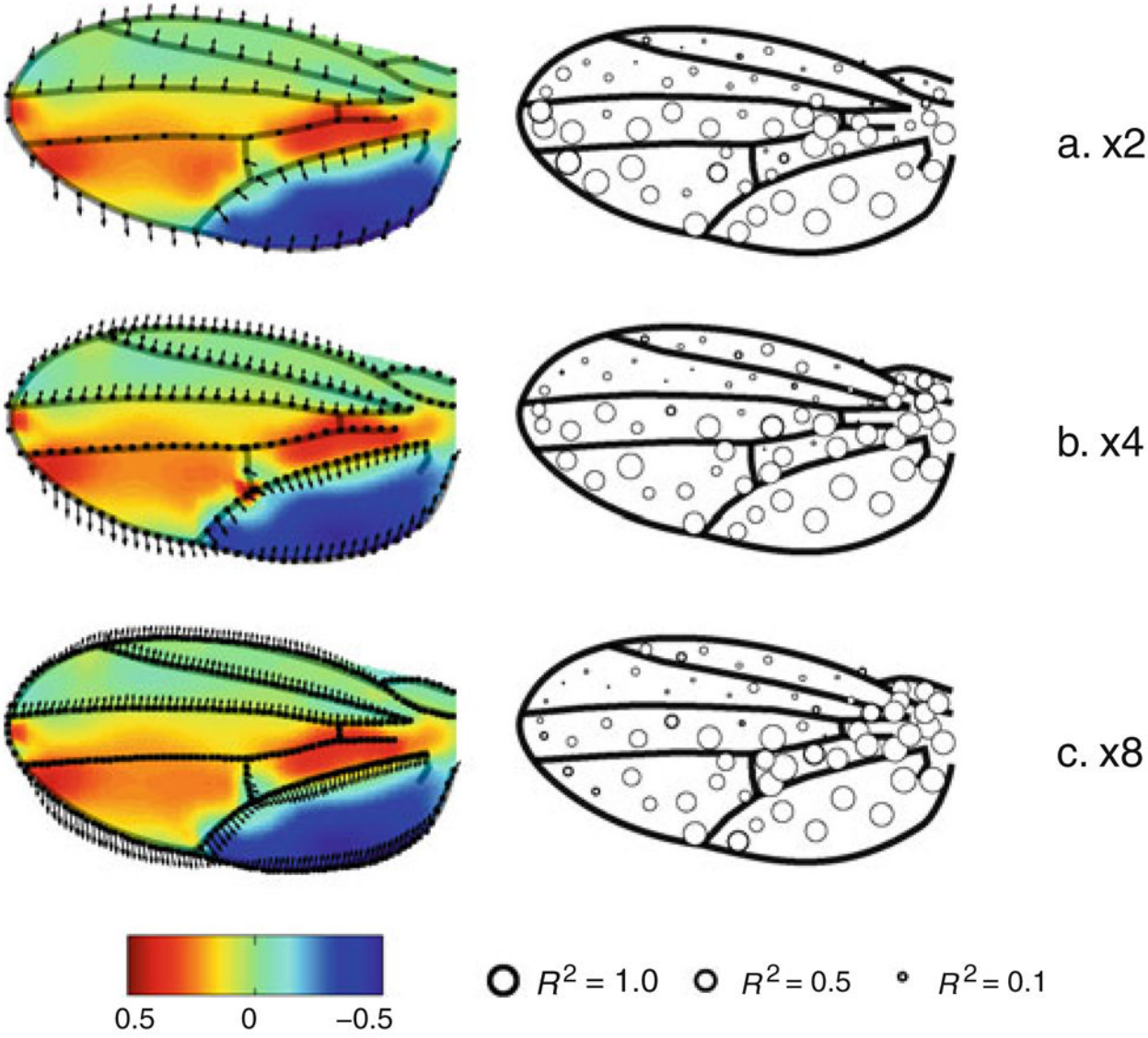

Fig. 7.

Effect of landmark sampling density on interpolation. Density multipliers with respect to original simulation study are 2 (**a**), 4 (**b**), and 8 (**c**). *Left column* shows heat maps of TPS interpolations of local changes in area based on each set of landmarks and semi-landmarks; *right column* shows R^2 values from univariate ANOVAs based on individual Jacobians, evaluated on a triangulated grid. Bubble diameters are proportional to average R^2 values and thickness of bubble edges are proportional to R^2 standard errors, computed from 100 tests of differences between two groups of $N = 50$ configurations each

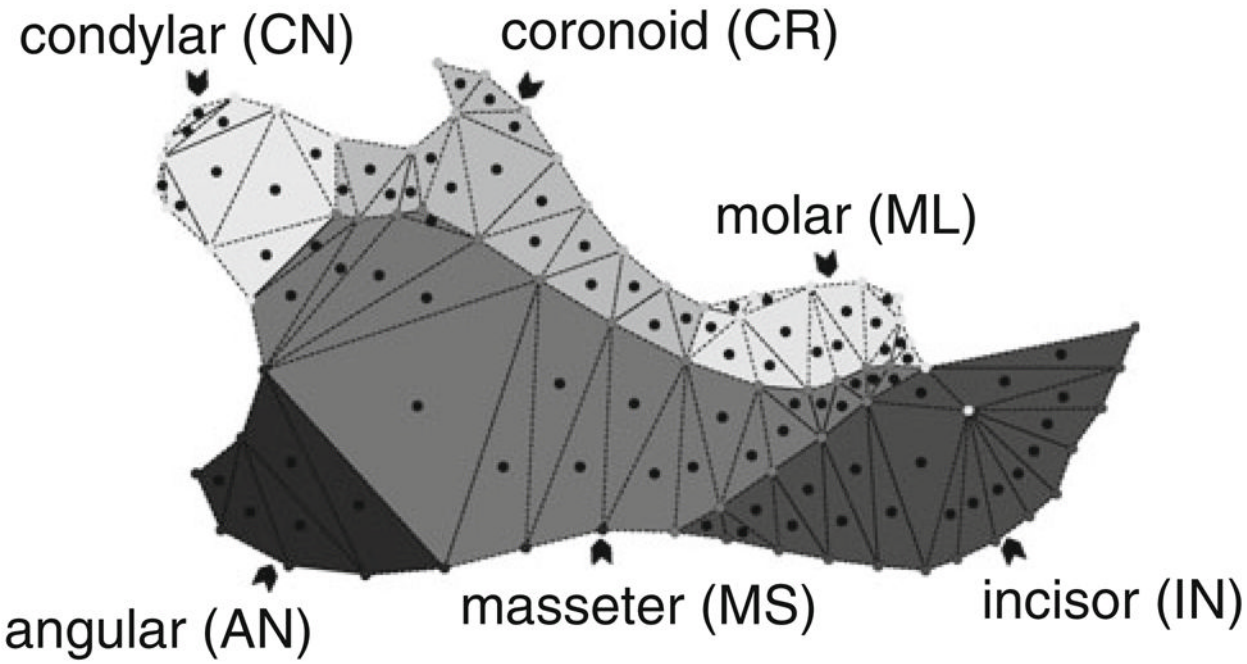

Fig. 8.

Triangulation and triangle centroid selection on a reference configuration of a rodent mandible. Triangulation based on landmarks and semi-landmarks (*grayed circles*); triangle centroids (*black circles*) indicate evaluation points for interpolation functions. Five partitions/modules discussed in text denoted by distinct *shades* of *gray*

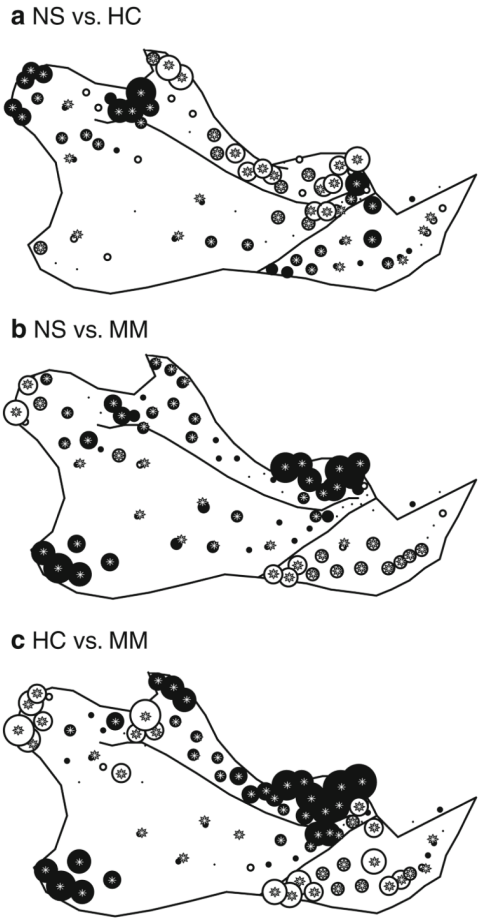

Fig. 9.

Pairwise differences in local shape between mandibles of three species of Sigmodontine rodents, mapped on a reference configuration. Bubble diameter is proportional to absolute differences in Jacobians, all drawn at the same scale. *Open* and *closed circles* represent different signs for differences. *Asterisks* represent significant comparisons, after Bonferroni adjustment. NS = *Nectomys squamipes*, HC = *Holochilus chacarius*, MM = *Microryzomys minutus*

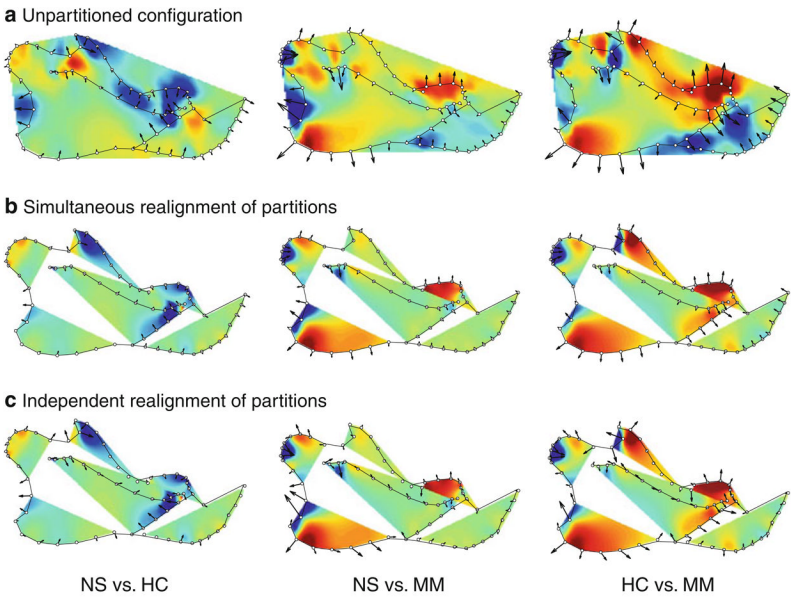

Fig. 10.

Pairwise differences in landmarks between mandibles of three species of Sigmodontine rodents, mapped on a reference configuration. **a** Differences based on full set of landmarks; **b** differences calculated without realigning landmarks. **c** Differences calculated after realigning landmarks within each of six partitions illustrated in Fig. 8. Note the local distortions in landmark orientation. Heat maps based on TPS interpolation of full set of landmarks (**a**) or individual partitions (**b**, **c**), with intensity denoting magnitude of local differences (legend as in Fig. 2). NS = *Nectomys squamipes*, HC = *Holochilus chacarius*, MM = *Microryzomys minutus*

Table 1

Percentages of sample variance explained by the main effect simulated in scenarios I and II depicted in Fig. 4 for Jacobian-, non-realigned- and realigned landmark data, with *P* values from corresponding MANOVAs in parentheses

Scenario	Sample	Original landmarks	Realigned landmarks	Jacobians
I	Whole configuration	99.99% (0.0001)		99.36% (0.0026)
	Partition L2	98.72% (0.0044)	99.29% (0.0023)	27.81% (0.1616)
	Partition L4-L5	99.93% (0.0002)	99.94% (0.0002)	98.06% (0.0066)
II	Whole configuration	99.99% (0.0001)		99.60% (0.0016)
	Partition L2	99.72% (0.0009)	99.80% (0.0006)	96.68% (0.0113)
	Partition L4-L5	99.93% (0.0002)	99.94% (0.0002)	98.30% (0.0058)

Jacobians were estimated as base-2 logarithms of determinants of Jacobian matrices derived from TPS functions

Table 2

Standardized variances of landmark- and Jacobian-based partitions in mandibles of three species of rodents

Partition	Species	Original landmarks[a]	Realigned landmarks[a]	Jacobians[b]
IN	NS	0.271	0.141	0.383
	HC	0.518	0.291	0.743
	MM	0.388	0.211	0.425
ML	NS	0.321	0.193	0.591
	HC	0.673	0.386	1.054
	MM	0.367	0.220	0.978
MS	NS	0.447	0.341	0.338
	HC	0.870	0.693	0.675
	MM	0.701	0.557	0.525
CR	NS	0.331	0.195	0.562
	HC	0.826	0.471	1.108
	MM	0.454	0.255	0.852
CN	NS	0.356	0.249	0.604
	HC	0.610	0.420	1.296
	MM	0.451	0.323	0.451
AN	NS	0.592	0.353	0.243
	HC	0.891	0.519	0.320
	MM	0.759	0.478	0.732

Jacobians were estimated as base-2 logarithms of determinants of Jacobian matrices derived from TPS functions. Variances were standardized by number of landmarks or Jacobian estimates. IN = incisor, ML = molar, MS = masseteric, CR = coronoid, and AN angular partitions; NS = *Nectomys squamipes*; HC = *Holochilus chacarius*; MM = *Microryzomys minutus*

[a] Multiplied by 1×10^5;

[b] Multiplied by 10

Table 3

RV-coefficient values for landmark- and Jacobian-based mandible partitions computed from data from three rodent species

Part	Species	Jacobians					Original partitions					Realigned partitions				
		IN	ML	MS	CR	CN	IN	ML	MS	CR	CN	IN	ML	MS	CR	CN
ML	NS	0.11					0.12					0.11				
	HC	0.09					0.28					0.17				
	MM	0.12					0.20					0.10				
MS	NS	0.22	0.15				0.31	0.14				0.18	0.17			
	HC	0.29	0.27				0.28	0.15				0.21	0.11			
	MM	0.31	0.28				0.21	0.16				0.12	0.13			
CR	NS	0.06	0.19	0.20			0.23	0.13	0.13			0.17	0.14	0.14		
	HC	0.18	0.32	0.23			0.15	0.15	0.14			0.09	0.21	0.13		
	MM	0.07	0.58	0.21			0.13	0.25	0.13			0.09	0.08	0.14		
CN	NS	0.11	0.08	0.07	0.10		0.18	0.15	0.18	0.23		0.15	0.17	0.10	0.20	
	HC	0.04	0.05	0.07	0.06		0.26	0.10	0.11	0.24		0.20	0.11	0.09	0.18	
	MM	0.09	0.06	0.10	0.19		0.10	0.12	0.12	0.24		0.11	0.11	0.12	0.14	
AN	NS	0.06	0.08	0.07	0.08	0.08	0.21	0.17	0.13	0.15	0.25	0.21	0.14	0.13	0.07	0.14
	HC	0.05	0.13	0.06	0.07	0.05	0.16	0.21	0.18	0.18	0.19	0.13	0.24	0.15	0.10	0.09
	MM	0.05	0.04	0.03	0.02	0.05	0.12	0.11	0.10	0.15	0.27	0.12	0.10	0.12	0.11	0.17

Jacobians were estimated as base-2 logarithms of determinants of Jacobian matrices derived from TPS functions. IN = incisor, ML = molar, MS = masseteric, CR = coronoid, and AN angular partitions; NS = *Nectomys squamipes*; HC = *Holochilus chacarius*; MM = *Microryzomys minutus*